ΕΘΝΙΚΟ ΜΕΤΣΟΒΙΟ ΠΟΛΥΤΕΧΝΕΙΟ

ΔΠΜΣ ΥΠΟΛΟΓΙΣΤΙΚΗΣ ΜΗΧΑΝΙΚΗΣ

ΣΧΟΛΗ ΧΗΜΙΚΩΝ ΜΗΧΑΝΙΚΩΝ

Buckling of frames and columns with initial imperfections

By Georgios Soimoiris

Academic Advisor: Lecturer Vissarion Papadopoulos

Buckling Analysis of Frames and Columns with Initial Imperfections

George Soimoiris

Diploma in Civil Engineering, NTUA

M.S. in Computational Mechanics, NTUA

CONTENTS

Acknowledgements

First of I would really like to thank my academic advisor Lecturer Vissarion Papadopoulos for his excellent guidance, unlimited concern and help that he provided me during the period of this work.

I would also like to thank Dominik Schillinger for sending me the power spectra data for the four meter long columns and the time he afforded me during his short stay in Athens for explaining me several issues on his diploma thesis and his interest for this work. Furthermore I would like to thank NTUA's PhD candidates Dimitris Savvas for helping me managing with Abaqus and Odysseas Kokkinos for sharing his office with me in the Lab of the Institute of Structural Analysis and Seismic Research of the School of Civil Engineering.

At last I would like to thank my parents, my sister and friends for their great love, support and criticism during all these years.

Georgios Soimoiris

Athens, October 2011

CHAPTER 1

INTRODUCTION

The wide usage of thin-walled slender steel members in constructions has made necessary the study of their behavior under any type and kind of loading. These members are preferred because they lead to leight-weightend constructions with more economic design and are proven to have a more efficient load-carrying behavior especially under bending.

The total strength of a thin-walled I-section can be easily affected by imperfections that are created in the web and the flanges during the manufacturing process, their transportation and the placement in the building site. These imperfections are classified in *geometric imperfections*, that refer to the deviation of the geometry from the perfect to the imperfect shape of the member, the *thickness imperfections* that refer to the changes from the nominal thickness and the so-called *material imperfections* that refer to the deviation of the material parameters (Young's modulus, Poisson's ratio etc.). Finally there are two more kinds of imperfections: the *residual stresses* that are local tension stresses around the web-flange junctions and are caused during the cooling process or after rolling and the *boundary imperfections* that refer to imperfections in support and loading conditions.

It is noticed that these imperfections lead to second order phenomena that reduce the load carrying capacity of the member under compression or/and bending and also reduce the critical buckling load. These reduces of the critical loads vary between nominally identical members. Many researchers have studied the influence of these imperfections, such as Becque and Rasmussen (2007), Degee et al. (2008), Schillinger and Papadopoulos (2008), Papadopoulos and Papadrakakis (2005) and others. Respectively in frames instability can be caused before any of the cross sections of the members misses by compression or bending or a combination of both. So, it is of important matter to investigate the behavior and the influence of imperfections upon the critical load that leads to instability.

1.1 Modeling of Imperfections

The determination of imperfections at each and every steel member is generally time-consuming and uneconomical. On the other hand, the assumption that imperfections can be described by deterministic values leads to non-reliable results, because they vary between identical members and take place in different combinations.

Many researchers in the past have suggested a stochastic approach of imperfections against the deterministic one. The main idea is that through a small specimen of measurements of imperfections of steel members a stochastic field can be generated, that represents possible values of imperfections. From these groups generated, a sample can be chosen through the Monte Carlo Simulation by entering in the perfect geometry. A combination of non-linear finite element method, advanced stochastic methods such as spectral representation and Monte Carlo Simulation has proven to be very effective in buckling analysis of imperfect members.

There are only two published articles that refer to the deterministic approach of imperfections of I-sections by Rasmussen and Hancock (1998,2000) and only a few that refer to the stochastic approach of imperfections and examine the behavior of shells and plates for variable values of several parameters such as height, width, thickness, Young's modulus etc. The most recent study that enters global and local imperfections in the geometry of thin-walled I-sections, thickness imperfections and residual stresses is Schillinger's (2008) and Schillinger and Papadopoulos (2008). In this study short length columns are examined under axial compression and bending in order to derive the stochastic interaction curve and the histogram that shows the variance of the critical buckling loads. There have also been published articles that refer to the buckling behavior of shells with random imperfections by Schenk and Schueller (2003), Stefanou and Papadrakakis (2004), Papadopoulos and Papadrakakis (2004,2005) and Papadopoulos and Iglesis (2007), while the general methodology has been described by Argyris et al. (2002). At last in Dinis and Camotim (2011) the local, distortional and global buckling loads of cold-formed steel U cross-section columns are defined taking under consideration initial geometric imperfections of 10% of the wall thickness and L/1000 on the global mode.

1.2 Scope of the Present Study

Scope of the present study is to determine the influence of local and global imperfections of a thin-walled I-section in buckling analysis of frames and columns. The members will be 4m long and the other geometric and material properties will be the same with those used in Schillinger (2008). A histogram of the critical buckling loads of columns and a histogram that shows the critical loads that lead to instability of frames are about to be determined.

A data base for the imperfections is provided by Hasham and Rasmussen (1997), which have measured the imperfections of 6 identical columns. Using the as above described power spectrum method on the real measurements and the Monte Carlo Simulations result imperfections that correspond to a more realistic approach of the shape of a member and so the results of the analysis are closer to the real behavior under any kind of boundary and loading conditions. The measurements refer to a 2m

long column, so by energy scaling they can be transformed to correspond on a 4m long column.

Based on these experimental data the appropriate stochastic model is being chosen in order to represent their stochastic properties. More specific, geometric imperfections are described as non-homogeneous Gaussian fields. Through a simple method that is based on the harmonic wavelet method and is described in Schillinger (2008) the evolutionary power spectra are estimated. After that, the spectrum representation method is applied for the digital sampling of imperfections.

CHAPTER 2

NON-LINEAR ANALYSIS

2.1 Introduction

Non-linear analysis is a very precise method that allows us to compute the inner forces, moments, displacements and rotations that develop in a construction under any type of loading and corresponds to its real behavior. As known, there are two types of non-linearity: material and geometric. The first one takes under account the plastic behavior of the material and the second one considers any kind of geometric imperfections as far as changes – distortions – from the perfect shape of the structure during the development of the loading.

The Finite Element Method, using the triangular shell element for the modeling of the structure's geometry and the Arc-Length Method for the solution of the non-linear equilibrium equations, represent a reliable method for the determination of the force-displacement curve for such kind of problems.

2.2 The triangular shell element

The triangular shell element is a 3-node element with 6 degrees of freedom at each node: three dimensional and three rotational at each axe. It combines the membranic behavior of a disk and the bending behavior of a plate and is based on the classic theory of thin shells, in which the transverse shearing displacement is ignored.

Generally, this kind of elements can be enrolled in the following categories:

1) Planar elements that combine the properties of a plain stress element and a plate element
2) Curved elements formulated by the classic theory of shells
3) Elements that result from the degeneration of three dimensional elasticity finite elements.

The combination of a triangular plate element and a triangular element of plain stress with transverse rotational degrees of freedom is proved to be very effective on the formulation of a planar triangular shell element with 18 degrees of freedom. So, the vector of displacements can be written as:

$$\{d'\} = \left\{[u_i][v_i][\theta_{zi}][w_i][\theta_{xi}]\left[\theta_{yi}\right]\right\}^t \qquad (2.1)$$

With i=1,2,3 denotes the 3 axes.

The stiffness matrix results from the combination of the two sub matrices k_m (membranic) and k_b (bending):

$$\underset{(18\times18)}{[k']} = \begin{bmatrix} [k_m] & [0] \\ [0] & [k_b] \end{bmatrix} \qquad (2.2)$$

2.3 The Arc Length Method

The Arc Length Method is inducted in the iterative Newton-Raphson Method that is used for the solution of non linear equations with many degrees of freedom and has the advantage to overcome critical points of the force-displacement curve and follow/attend instable branches of equilibrium (snap back, snap through).

The Newton-Rapshon Method then takes the form:

$$\underset{\sim}{K}_T\left(\underset{\sim}{x}_k\right)\cdot\underset{\sim}{u} = -\underset{\sim}{r}\left(\underset{\sim}{x}_k\right), \underset{\sim}{x}_{k+1} = \underset{\sim}{x}_k + \underset{\sim}{u} \qquad (2.3)$$

where: $\underset{\sim}{r}\left(\underset{\sim}{x}_k\right) = \underset{\sim}{F}\left(\underset{\sim}{x}_k\right) - \underset{\sim}{R}$

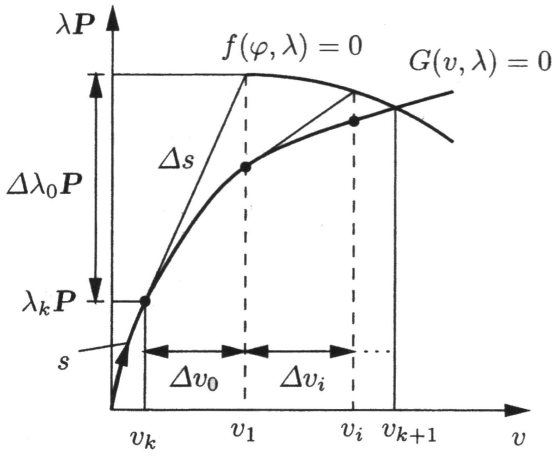

Fig. 2.1 *The Arc Length Method.*

The value of the external load is being controlled by a coefficient λ, in order to converge the solutions in instable regions of the equilibrium curve, so that:

$$\underset{\sim}{r}\left(\underset{\sim}{x},\lambda\right) = \underset{\sim}{F}\left(\underset{\sim}{x},\lambda\right) - \lambda\cdot\underset{\sim}{\bar{R}} \qquad (2.4)$$

$\underset{\sim}{\bar{R}} \rightarrow$ representable load vector

The incrementing loading within an iteration in the step i is:

$$\Delta \underset{\sim}{\bar{R}} = \Delta\lambda \cdot \underset{\sim}{R} \ , \ \Delta\lambda = \lambda - {}^{i}\lambda \tag{2.5}$$

And the respective increment of displacement is:

$$\Delta \underset{\sim}{x} = \underset{\sim}{x} - {}^{i}\underset{\sim}{x} \tag{2.6}$$

Spherical arc length from which Δλ results:

$$\Delta \underset{\sim}{x}^{T} \Delta \underset{\sim}{x} + \Delta\lambda^{2} \psi^{2} \underset{\sim}{\bar{R}}^{T} \underset{\sim}{\bar{R}} = s^{2} \tag{2.7}$$

Where s is the value of the generalized vector:

$$\underset{\sim}{s} = \begin{Bmatrix} \Delta \underset{\sim}{x} \\ \Delta\lambda\psi \underset{\sim}{\bar{R}} \end{Bmatrix} \tag{2.8}$$

Based on the above, the Newton-Raphson Method can be formulated as:

$$\underset{\sim}{\underline{K}}_{T}\left(\underset{\sim}{x}_{k}\right) \cdot \underset{\sim}{u}_{k+1} = \text{-}\underset{\sim}{r}\left(\underset{\sim}{x}_{k}, \lambda_{k+1}\right) \tag{2.9}$$

where:

$$\underset{\sim}{r}\left(\underset{\sim}{x}_{k}, \lambda_{k+1}\right) = \underset{\sim}{F}\left(\underset{\sim}{x}_{k}\right) - \left[\underset{\sim}{F}\left(\underset{\sim}{x}_{k}\right) + \gamma_{k} \underset{\sim}{\bar{R}}\right] \tag{2.10}$$

$$\begin{aligned} &\underset{\sim}{x}_{k+1} = \underset{\sim}{x}_{k} + \underset{\sim}{u}_{k+1}, \Delta \underset{\sim}{x}_{k+1} = \Delta \underset{\sim}{x}_{k} + \underset{\sim}{u}_{k+1} \\ &\lambda_{k+1} = \lambda_{k} + \underset{\sim}{\gamma}_{k}, \Delta\lambda_{k+1} = \Delta\lambda_{k} + \underset{\sim}{\gamma}_{k} \end{aligned} \tag{2.11}$$

Combining the above equations comes up a second order equation of the form:

$$a_{1}\gamma_{k}^{2} + a_{2}\gamma_{k} + a_{3} = 0 \tag{2.12}$$

with coefficients:

$$\begin{aligned} a_{1} &= \left(\underset{\sim}{u}'_{k+1}\right)^{T} \underset{\sim}{u}'_{k+1} + \psi^{2} \underset{\sim}{\bar{R}}^{T} \underset{\sim}{\bar{R}} \\ a_{2} &= 2\left(\underset{\sim}{u}''_{k}\right)^{T} \left(\Delta x_{k} + \underset{\sim}{u}'_{k+1}\right) + 2\Delta\lambda_{k}\psi^{2} \underset{\sim}{\bar{R}}^{T} \underset{\sim}{\bar{R}} \\ a_{3} &= \left(\underset{\sim}{u}''_{k+1}\right)^{T} \left(2\Delta x_{k} + \underset{\sim}{u}''_{k+1}\right) \end{aligned} \tag{2.13}$$

and from which result the two solutions : $\gamma_{k}^{(1)}, \gamma_{k}^{(2)}$

that define the generalized vectors : $\underset{\sim}{S}_{k}^{(1)}, \underset{\sim}{S}_{k}^{(2)}$.

As a solutions is being chosen the one that forms the smallest angle θ with the generalized vector $\underset{\sim}{S}_{k}$:

$$\cos\vartheta^{(j)} = \frac{\underset{\sim}{S}_k^T \underset{\sim}{S}_{k+1}^{(j)}}{s^2} \qquad (2.14)$$

where:

$$\underset{\sim}{S}_k = \begin{Bmatrix} \Delta\underset{\sim}{x}_k \\ \Delta\lambda_k \psi \underset{\sim}{\bar{R}} \end{Bmatrix}, \underset{\sim}{S}_{k+1}^{(j)} = \begin{Bmatrix} \Delta\underset{\sim}{x}_k + \underset{\sim}{u}_{k+1}^{(j)} \\ \left(\Delta\lambda_k + \gamma_k^{(j)}\right)\psi \underset{\sim}{\bar{R}} \end{Bmatrix} \qquad (2.15)$$

With parameter ψ taking the values 0 or 1.

2.4 Von Mises Plasticity

For the inelastic analysis of a structure it is necessary to define a yield criterion. The von Mises criterion is described by the axial strain yield stress σ_y and the second deviatoric stress invariant J_2.

If σ_1, σ_2, σ_3 are the main stresses and the hydrostatic component is equal to:

$$\sigma_m = \frac{\sigma_1 + \sigma_2 + \sigma_3}{3} \qquad (2.16)$$

Then, the divergent stresses are given by the relation:

$$\sigma'_{ij} = \sigma_{ij} - \delta_{ij}\sigma_m \qquad (2.17)$$

From which the second deviatoric stress invariant J_2 can be computed as:

$$J_2' = \frac{1}{2}\left(\sigma_1'\right)^2 + \left(\sigma_2'\right)^2 + \left(\sigma_3'\right)^2 = \frac{1}{6}\left[\left(\sigma_2 - \sigma_3\right)^2 + \left(\sigma_3 - \sigma_1\right)^2 + \left(\sigma_1 - \sigma_2\right)^2\right] \qquad (2.18)$$

The von Mises criterion can be formulated as:

$$f_y^M = \left(\sigma_1 - \sigma_2\right)^2 + \left(\sigma_2 - \sigma_3\right)^2 + \left(\sigma_3 - \sigma_1\right)^2 - \sqrt{2}\sigma_y = 0 \qquad (2.19)$$

The geometric representation of this criterion is shown in the Figure 2. … and represents a cylinder around the axis $\sigma_1=\sigma_2=\sigma_3=0$. Alternative, by using the second derivative of the diverge tensor of the stresses it results:

$$f_y^M = J_2' - \frac{1}{3}\sigma_y{}^2 = 0 \qquad (2.20)$$

The von Mises yield criterion considers that the wastage happens when the second derivative of the divergent tensor of the stresses in multiaxial tension becomes equal to this in uniaxial and therefore it is also known as J_2' plasticity.

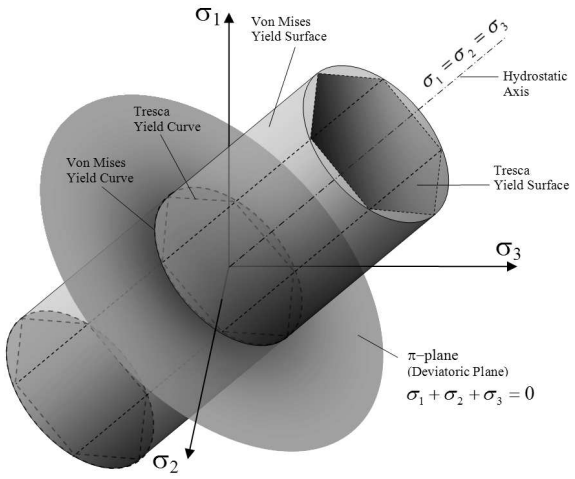

Fig. 2.2 *Cylindrical von-Mises yield surface in the principal stress space.*

2.5 Non-linear Analysis using *ABAQUS*

Abaqus gives the opportunity of running a material and geometric non-linear model using the as above described Arc Length Method through the *STATIC, RIKS command available by increasing the loads that act on the structure until it becomes instable. Through this procedure the critical load can be obtained and furthermore the displacements, rotations and stresses.

The geometry - described by the nodal coordinates, that have resulted by the stochastic analysis - the connectivity matrix, the properties of the material, the external forces and the supports are given through an input file (*.inp). Then follows the non-linear analysis and at last the results that are stored in an *.odb file automatically by the program. From this file we obtain the results of our interest to compose the force-displacement curve and establish the critical buckling load.

Abaqus has the ability to solve non-linear equations through a number of non-linear iterations that are given by the user, depending on the desirable precision.

The finite element used for the analysis is the shell element S3 available in Abaqus. It is also cited sententiously that the geometry is given by the coordinates of the nodes that have occurred by the discretization of the structure and these nodal coordinates differ for every Monte Carlo Simulation. More information is given in Chapters 3 and 4.

CHAPTER 3

STOCHASTIC FEM

3.1 Introduction

Stochastic FEM represents a combination of two important methods that are used for the solution of complicated problems of modern mechanics:

a) The finite element method and
b) The stochastic analysis

As known, the Finite Element Method is the quickest, most reliable and effective method for the solution of complicated problems of mechanics with the assistance of computer. This method can handle problems with complex geometry, while it has the ability to take under consideration the material and geometric non-linearities. One the other hand, the stochastic analysis allows us to manage numerically many uncertainties, videlicet parameters whom the exact values are unknown – such as for example the alteration of Young's modulus or the variation of the area of a cross-section, the wind and seismic loads, the geometric imperfections of a member etc. – and are not taken into account in the deterministic analysis. The variability of these values may cause effects on the structure's response and must be entered in the computations.

The uncertainties of these parameters are simulated as stochastic fields (stochastic procedures in space), are entered in the analysis and then the variance of the response is being computed. The method of Stochastic FEM is based on the representation of the stochastic as a random numbers series. One of the already known methodologies to manage this kind of problems is the spectral representation method, combined with the Monte Carlo Simulation (MCS).

3.2 Stochastic Fields

Every function, whose variables' values are random variables, is called stochastic. Examples of stochastic functions are the area of a cross-section, the wind and seismic loading, the imperfections of a structure, the temperature etc. the difference between them and real functions relies on the fact that stochastic functions consist of a set of sample-functions and are not univocal.

Stochastic functions are called stochastic procedures, if their variables tie up with time, and stochastic fields, if their variables refer to space. In the case of a structure's geometric imperfections the clause 'stochastic fields' is used.

A continuous variable Y is a function, when for every real number y there is a probability P[Y<y], whose distribution is given by a density probability function. A random variable Y is called Gaussian if its density probability function is of the form:

$$p(y) = \frac{1}{\sqrt{2\pi}} \exp\left[\frac{(y-\mu)^2}{2\sigma^2} \right] \qquad (3.1)$$

Where μ is mean value and σ the standard deviation. Gauss distribution – or also normal distribution – is very important, because of the central limit theorem, which is very useful in our study.

A stochastic field *f(x)* can be considered as a random variables series $f(x_1)$, $f(x_2),\ldots,f(x_n)$, while it can also be easily managed statistically. This means that a stochastic field can be considered as a function of a deterministic variable *x*, whose results are random variables.

A stochastic field can be mathematically described by the multidimensional summative probability function:

$$F(x_1,\ldots,x_n)\,dx_1\ldots dx_n = P\left\{ x_1 \le f(x_1) \le x_1 + dx_1 \,|\ldots|\, x_n \le f(x_n) \le x_n + dx_n \right\} \qquad (3.2)$$

Which can be mathematically approximated by two functions:

a) the mean value

$$\mu_f(x) = E\left[f(x) \right] = \int_{-\infty}^{+\infty} f \cdot p(f,x)\,df \qquad (3.3)$$

b) and the autocorrelation function:

$$R_{ff}(x_1,x_2) = E\left[f(x_1) f(x_2) \right] = E\left[f_1 f_2 \right] = \int_{-\infty}^{+\infty}\int_{-\infty}^{+\infty} f^2 \cdot p^*(f_1,x_1;f_2,x_2) \qquad (3.4)$$

Instead of the autocorrelation function, most commonly is used the autocovariance function that refers to the variance of a random variable:

$$K_{ff}(x_1,x_2) = E\left\{ \left[f(x_1) - \mu_f(x_1) \right] \cdot \left[f(x_2) - \mu_f(x_2) \right] \right\} = E\left[f_1 \cdot f_2 \right] - \mu_f(x_1) \cdot \mu_f(x_2)$$
$$= \int_{-\infty}^{+\infty}\int_{-\infty}^{+\infty} f^2 \cdot p^*(f_1,x_1;f_2,x_2) - \mu_f(x_1) \cdot \mu_f(x_2) \qquad (3.5)$$

A stochastic field *f(x)* can be expressed as the sum of a zero-mean stochastic field and its mean function *μ(x)*, then the stochastic field:

$$g(x) = f(x) - \mu_f(x) \qquad (3.6)$$

Will have a zero mean function and will keep the statistical properties of the field *f(x)*.

Stationary are called the stochastic fields for whom the multidimensional summative probability function does not change its value, which mean that:

$$\mu_f(x) = \mu_f, \sigma_f(x) = \sigma_f \qquad (3.7)$$

The fact that the mean and the standard deviation of these fields are constant and independent from the variable *x* leads us to the following conclusion:

$$\begin{aligned} R_{ff}(x_1, x_2) &= R_{ff}(x_1, x_1 + \tau) = R_{ff}(\tau) = R_{ff}(-\tau) \\ K_{ff}(x_1, x_2) &= K_{ff}(x_1, x_1 + \tau) = K_{ff}(\tau) = K_{ff}(-\tau) \end{aligned} \qquad (3.8)$$

And:

$$\sigma_f^2(x) = K_{ff}(0) \qquad (3.9)$$

$$K_{ff}(\tau) \to 0, \tau \to \infty \qquad (3.10)$$

A stochastic field is called ergodic when the mean function and the autocorrelation function of the sample are identified with the mean value and the autocorrelation function of the whole set. This means that the mean function of a sample is identified with the mean function of all the samples of the set, as seen in the *Fig.3. … .*

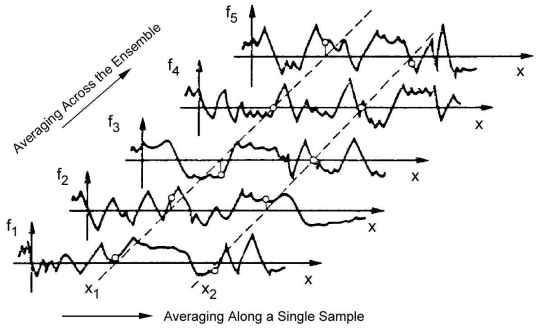

Fig. 3.1 *Μέση τιμή κατά μήκος ενός δείγματος και συνολική μέση τιμή.*

Frequency Analysis

Frequency or Fourier analysis is a power tool for solving engineering problems by transforming a random field to a frequency spectrum through Fourier transform:

$$\bar{f}(\omega)=\frac{1}{2\pi}\int_{-\infty}^{+\infty} f(x)e^{-i\omega x}dx \qquad (3.11)$$

While the inverse Fourier transform is:

$$f(x)=\int_{-\infty}^{+\infty} \bar{f}(\omega)e^{i\omega x}d\omega \qquad (3.12)$$

The analytical evaluation of the above integrals is genrally veru difficult, if not possible, and so there are usually used discrete Fourier transforms such as the fast Fourier transform (FFT).

Applying the Fourier transform on the autocorrelation function we obtain the power spectra density function, also known as power spectrum:

$$S_{ff}(\omega)=\frac{1}{2\pi}\int_{-\infty}^{+\infty} R_{ff}(\tau)e^{-i\omega x}d\tau \qquad (3.13)$$

And by applying the inverse Fourier transform we obtain:

$$R_{ff}(x)=\int_{-\infty}^{+\infty} S_{ff}(\tau)e^{-i\omega x}d\tau \qquad (3.14)$$

Because the autocprrelation function is even it can be written as:

$$S_{ff}(\omega)=\frac{1}{2\pi}\int_{-\infty}^{+\infty} R_{ff}(\tau)\cos(\omega\tau)d\tau \qquad (3.15)$$

To the effect that the power spectrum is y-symmetric it is called two-sided. It is always also positive defined and therefore it can represent the energy function of the imperfect geometry. It has also been proved that there can be defined an upper limit of the frequency, beyond which the power spectrum can be considered as zero, due to its small contribution.

In the case of stochastic zero mean fields we have that:

$$E\left[f^2(x)\right]=R_{ff}(0)=\int_{-\infty}^{+\infty} S_{ff}(\omega)d\omega=\sigma_f^2 \qquad (3.16)$$

In this study, that deals with geometric imperfections, where the stochastic filed f(x) represents the imperfect geometry of a member from its perfect geometry, we have two categories:

- If the stochastic field is homogeneous then the power spectrum is relative only to the frequency ω: S(ω).

- If the stochastic field is non-homogeneous then the power spectrum is of the form: S(ω,x).

  In the case of the non-homogeneous stochastic fields the computation of the power spectrum S(ω,x) is very difficult by using the Fourier transform, so another method is used, that is described by Schillinger 2008 and is called Wavelet-based Estimation of the Power Spectrum.

3.3 Monte Carlo Simulation

In the present study, the Monte Carlo Simulation is used in order to carry out a large number of iterated solutions with the Finite Elements Method – taking into account randomly every time a different sample of geometric imperfections – that compute the limit stability loading.

Because of the random value of the imperfections, the limit load differs at each MCS. By using the spectral representation method, there can be many specimens of imperfections through the experimental measurements produced, in order to create a data space, from which a sample is being randomly selected at every MCS. For every MCS we obtain a different limit load. The whole number of the limit load values constitute the result of the stochastic procedure.

Monte Carlo Simulation is used for solving many kinds of problems through random or pseudo-random numbers, videlicet through a statistical procedure, which numbers are considered as independent variables with the same possibility in the space [0,1]. The vocable “simulation” means the sampling experiments on the model of a physical system, which model represents the geometric and mechanical properties of the system with finite numerical data, so that they can be administrated by computing means. Because of the big computing effort needed to solve such kinds of problem, there have been many sampling techniques developed that increase the effectiveness of the method and decrease statistical error. Consequently, the number of simulations needed reduces for the same statistical precision. These techniques are also called dispersion reducing techniques.

Spectral representation method

The methods that are used for the simulation of stochastic fields are those with a series of discretized random variables (point discretization, local average,

interpolation and series development) or methods of producing sampling functions, such as spectral representation method.

The geometric imperfections of a member can be generally considered as stochastic fields. Through this methodology, homogeneous samples can be generated, that will be used as data for the Monte Carlo Simulation.

More specifically, there can be generated many imperfection functions $f^{(i)}(x)$ through the already known power spectra functions $S(\omega)$ and $S(\omega,x)$ of the $f(x)$ functions – that have been generated by the experimental measurements of the 6 samples – through the equation:

$$\hat{f}(x) = \sqrt{2}\sum_{n=0}^{N-1} A_n \cos(\omega_n x + \varphi_n) \qquad (3.17)$$

Where:

$$A_n = \sqrt{2S(\omega_n)\Delta\omega}, n = 0,1,...,N-1$$
$$\omega_n = n\Delta\omega, n = 0,1,...,N-1$$
$$\Delta\omega = \frac{\omega_{up}}{N}$$
$$A_0 = 0, S(\omega_0 = 0) = 0$$

It has already been cited that the parameter ω_{up} refers to an upper limit of the frequency, beyond which the autocorrelation function is supposed to be zero. Parameter ϕ_n expresses random phase angles and takes values in the field $[0,2\pi]$ so that:

$$p(\varphi_n) = \begin{cases} 1/2\pi, 0 \le \varphi_n \le 2\pi \\ 0, else \end{cases} \qquad (3.18)$$

The as above described method can also be applied on non-stationary stochastic fields, for which the power spectrum function is dependent from frequency and space, by substituting the $S(\omega_n)$ function with the $S(\omega_n,x)$.

Chapter 4

ESTIMATION OF EVOLUTIONARY POWER SPECTRA

4.1 Introduction

As already known, the evolutionary power spectra of global imperfections are non-homogeneous random fields with two variables: the spatial variable x and the frequency ω. In order to estimate this kind of power spectra, a wavelet theory has been developed, which then applied to the geometric imperfection data gives us the evolutionary power spectra S(ω,x).

4.2 Harmonic Wavelet Analysis

According to the wavelet transform a single mother wavelet function is being dilated and then translated in space in a basis of orthogonal functions. Through the parameter a, that controls the frequency, dilation is achieved and through parameter b spatial translation is achieved. This transform has a benefit on Fourier analysis, which uses a single function of a single spatial content x, because it can distinguish local events at different locations at the same frequency, see Schillinger (2008).

The general form of the wavelet transform of a process f(x) is:

$$w(a,b) = \frac{1}{\sqrt{a}} \int_{-\infty}^{+\infty} f(x)\psi^* \left(\frac{x-b}{a} \right) dx \qquad (4.1)$$

Where:

ψ(x) → the mother wavelet

w(α,b) → the wavelet coefficient at scale α and spatial position b

(*) → complex conjugation

While the imperfection signal f(x) is known, our first purpose is to choose a suitable for our case mother wavelet, which meets certain criteria, from a variety of mother wavelets mentioned in global bibliography. Newland has developed the harmonic wavelet transform w(x) for the estimation of power spectra, whose mother wavelet is:

$$W(\omega)=\begin{cases}1/2\pi, 2\pi \le \omega \le 4\pi \\ 0, elsewhere\end{cases} \qquad (4.2)$$

and has occurred by the Fourier transform of w(x). Applying the inverse Fourier transform on the mother wavelet we obtain the harmonic wavelet representation as follows:

$$w(x)=\int_{-\infty}^{+\infty} W(\omega)e^{i\omega x}dx \qquad (4.3)$$

and consists of a real and an imaginary part, shown in Fig……..

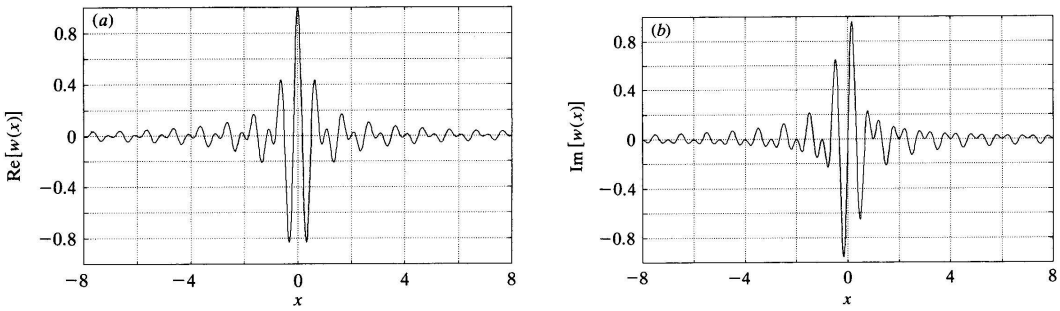

Fig. 4.1 *Real and imaginary part of the mother wavelet.*

The generalized harmonic wavelet, on the basis of the mother wavelet, in the frequency domain is defined as:

$$W_{(m,n),k}(\omega)=\begin{cases}\dfrac{1}{2\pi(n-m)}e^{\frac{-i\omega k}{nm}}, m2\pi \le \omega \le n2\pi \\ 0, elsewhere\end{cases} \qquad (4.4)$$

Where the scale (m,n) represents the frequency dilation and position k represents the spatial translation.

The complex harmonic wavelet coefficients of f(x) are:

$$a_{(m,n),k}=(n-m)\int_{-\infty}^{+\infty} f(x)w^*\left(x-\frac{k}{n-m}\right)dx \qquad (4.5)$$

Because of the orthogonality between the mother wavelets that correspond to different scales (m,n) and wavelets of the same scale at different positions k, the imperfection signal can be written as:

$$f(x)=\sum_{m,n}\sum_{k=-\infty}^{+\infty} a_{(m,n),k}w_{(m,n)}\left(x-\frac{k}{n-m}\right)+a^*_{(m,n),k}w^*_{(m,n)}\left(x-\frac{k}{n-m}\right) \qquad (4.6)$$

Where the first Σ denoted summation over pairs (m,n).

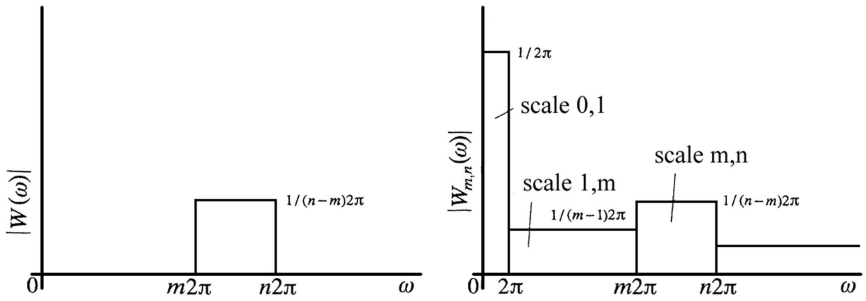

Fig. 4.2 *Single and Complex Harmonic Wavelet.*

4.3 Wavelet Based Estimation of Evolutionary Power Spectra

A non-homogeneous random field f(x) can be expressed using its harmonic wavelet coefficients $\alpha_{(m,n),k}$ as:

$$f(x)=2\sum_{k=0}^{n-m-1}\sum_{n,m}\left|a_{(m,n),k}\right|\frac{\sin\left(\pi(n-m)\left(x-\frac{k}{n-m}\right)\right)}{\pi(n-m)\left(x-\frac{k}{n-m}\right)}\cos\left(\pi(n+m)\left(x-\frac{k}{n-m}\right)+\phi_{(m,n),k}\right) \tag{4.7}$$

Where:

$\phi_{(m,n),k}$ → random phase angles

and

$$x=\frac{\hat{x}}{NT},\omega=\frac{\hat{\omega}}{NT}$$

are the dimensionless space and frequency, where N is the number of sample points and T is the sampling period of the imperfection signal.

The non-normalized local spectrum is of the form:

$$H_{(m,n),k}=4E\left[\left|a_{(m,n),k}\right|^2\right] \tag{4.8}$$

Where:

E → the operator of mathematical expectation

The normalized local spectrum of the generalized harmonic wavelet scheme is:

$$S_{(m,n),k}=\frac{4E\left[\left|a_{(m,n),k}\right|^2\right]}{n-m} \tag{4.9}$$

And is defined in the regions:

$$\begin{cases} m2\pi\le\omega\le n2\pi \\ \dfrac{k}{n-m}\le x\le\dfrac{k+1}{n-m} \end{cases}$$

The as above described method has been compared by Schillinger (2008) to the exact evolutionary spectrum which is of the form:

$$S(\omega,x)=S_{\text{hom}}(\omega)*g(x) \qquad (4.10)$$

Where in the place of $S_{hom}(\omega)$ has been used the homogeneous Kanai-Tajimi spectrum $S_{KT}(\omega)$ and g(x) is a specific envelope function.

The results of the performing test can be seen in the next Fig. 4.3:

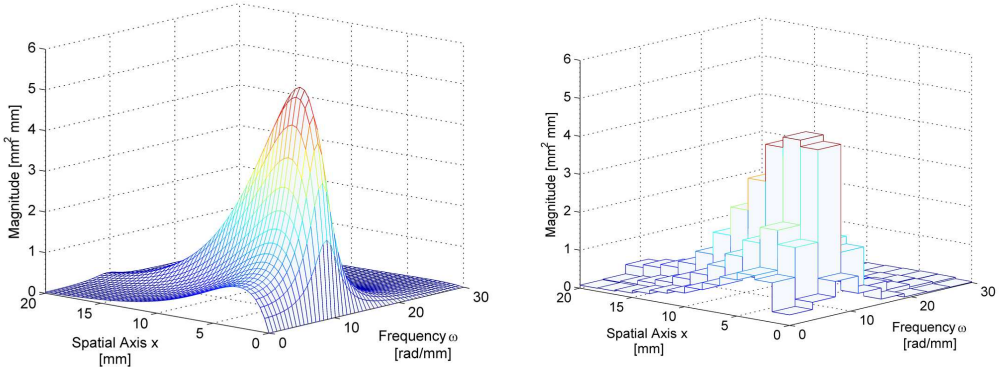

Fig. 4.3 *Exact and Harmonic Wave Based Estimate of Evolutionary Power Spectrum.*

This performance test has proved that the wavelet based estimation of power spectra approximates the evolutionary trend from the exact solution (5.10) really well.

It has been proved through the instantaneous mean square values:

$$\chi(x)=\int_{-\infty}^{+\infty}S(\omega,x)dx=E\left[\left|f(x)\right|^2\right]=\frac{1}{n-1}\sum_{i=1}^{n}f_i(x)^2 \qquad (4.11)$$

that the generalized harmonic wavelet scheme can detect changes of the energy across the spatial content x and approximately preserves the energy of the process, see Fig 4.4. The only disadvantage of the method lies on the discretization of the space-frequency domain, which cannot be small in both domains at the same time. This means that small changes in the space domain lead to large in the frequency one and reversely.

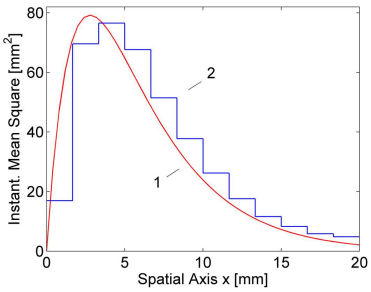

Fig. 4.4 *Instantaneous Mean Square of the Exact (1) and Estimated (2) Power Spectra.*

4.4 Estimation of Evolutionary Power Spectra of Separable Random Fields

It has already been mentioned that the Wavelet Based Estimation of Power Spectra cannot reach great accuracy in both space and frequency simultaneously. Schillinger and Papadopoulos (2009) make the assumption that the power spectra referred to the geometric imperfections can be handled as separable processes. This method was developed in order to handle the space and frequency resolution separable, in order to accomplish better accuracy. This assumption is based on the fact that the input files $f^{(i)}(x)$ of geometric imperfections represent separable or approximately separable random fields. According to the above, the power spectrum can be defined with the method of separation as:

$$S(\omega,x)=S(\omega)\cdot g(x) \qquad (4.12)$$

In order to estimate the evolutionary power spectrum from Eq. (4.12) , group of pairs [S',g'] can be arbitrarily chosen, so that they can satisfy the original components [S,g]:

$$\begin{aligned} S'(\omega)&=\lambda\cdot S(\omega)\\ g'(x)&=\frac{1}{\lambda}g(x) \end{aligned} \qquad (4.13a,b)$$

Where λ is an arbitrary positive number.

Eq. (4.13a,b) constitute sets of geometrically similar functions. This means that the relative shapes of the curves remain the same, but the area under these curves, that indicates the energy component, varies by the scaling factor λ. In the method of separation the spectrum component of Eq. (4.13a) is chosen as the homogeneous Fourier power spectrum:

$$S_h(\omega)=\frac{1}{L}\cdot\int_0^L S(\omega,x)\,dx=\lambda_h\cdot S(\omega) \qquad (4.14)$$

The function $g_h(x)$ can be obtained from Eq. (4.13b) by factor:

$$\lambda_h=\frac{1}{L}\cdot\int_0^L g(x)\,dx \qquad (4.15)$$

And so, the evolutionary power spectrum is decomposed into:

$$S(\omega,x)=S_h(\omega)\cdot g_h(x) \qquad (4.16)$$

An estimate of the homogeneous Fourier power spectrum $S_h(\omega)$ can be obtained from the periodogram of a series of samples $f^{(i)}(x)$:

$$\overline{S}_h(\omega) = E\left[\frac{1}{2\pi L}\left|\int_0^L f^{(i)}(x)\cdot w\left(x-\frac{L}{2}\right)\cdot e^{-i\omega x}dx\right|^2\right] \qquad (4.17)$$

An estimate of the spatial envelope g(x) can be obtained by the mean square of samples $f^{(i)}(x)$, which is:

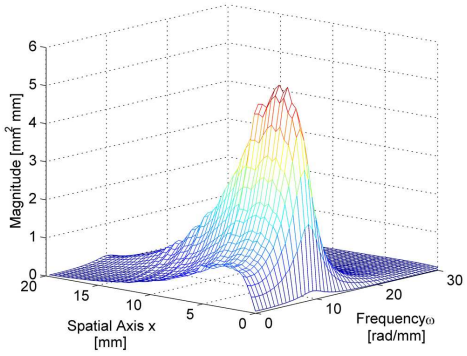

Fig. 4.5 *Evolutionary Power Spectrum generated by the method for separable processes.*

4.5 Evolutionary Power Spectra of Global and Local Imperfections

According to the methods that have been described in this – for non-homogeneous random fields – and the previous – for homogeneous random fields - chapter for the estimation of the evolutionary power spectra, it is time to extract these of our interest for the 4m long columns.

For the global imperfections it has been used the previous method for separable processes (4.12), where the normalized spectrum $S_{hom}^{*}(\omega)$ has been calculated by the Fourier transform and the normalized envelope $g^{*}(x)$ by the wavelet based estimation.

For the local imperfections the homogeneous power spectrum has been estimated by the following formula (Papadopoulos and Papadrakakis 2008):

$$S(\omega) = E\left[\frac{1}{L_0}\cdot\left|\int_0^L f(x)e^{-i\omega x}dx\right|^2\right] \qquad (4.13)$$

The length of the column is supposed to be L_0=4,00m=4000mm and for local imperfections the space domain has been discretized in 8192 points and the frequency domain in 512 with upper limit ω_{up}=0.0502, as shown in Fig. 4.6. The estimated power spectra, according to (4.13) are shown in Fig. 4.7 and Fig. 4.8.

For global imperfections, the space domain has been discretized in 2048 points and the frequency domain in 512, while ω_{up}=0.0125, as shown in Fig. 4.9. At last evolutionary power spectra S(ω,x) are shown in Fig. 4.10.

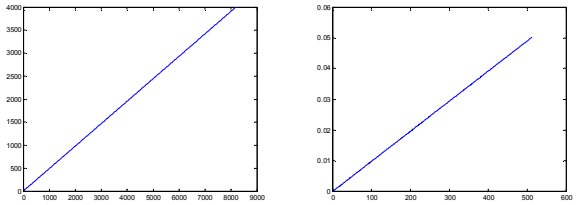

Fig. 4.6 *Space and frequency domains discretization for local imperfections.*

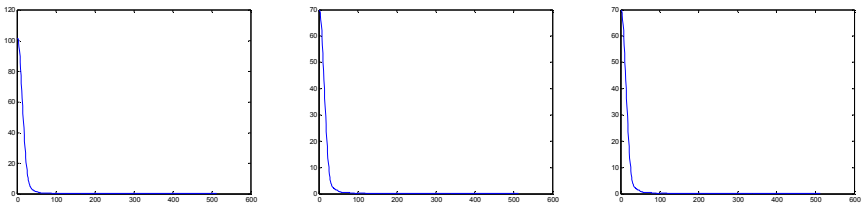

Fig. 4.7 *Power spectra of local imperfections δ_1, δ_2, δ_3.*

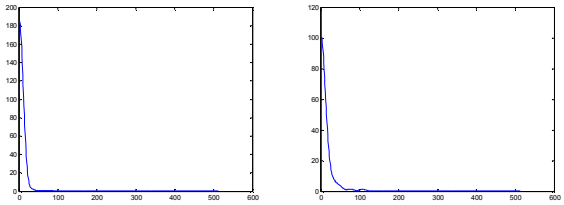

Fig. 4.8 *Power spectra of local imperfections δ_4, δ_5.*

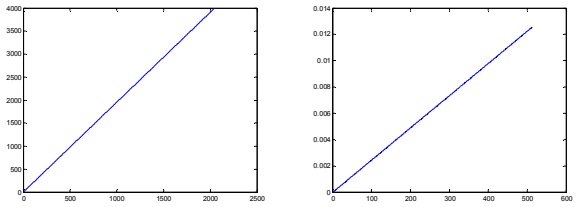

Fig. 4.9 *Space and frequency domains discretization for global imperfections.*

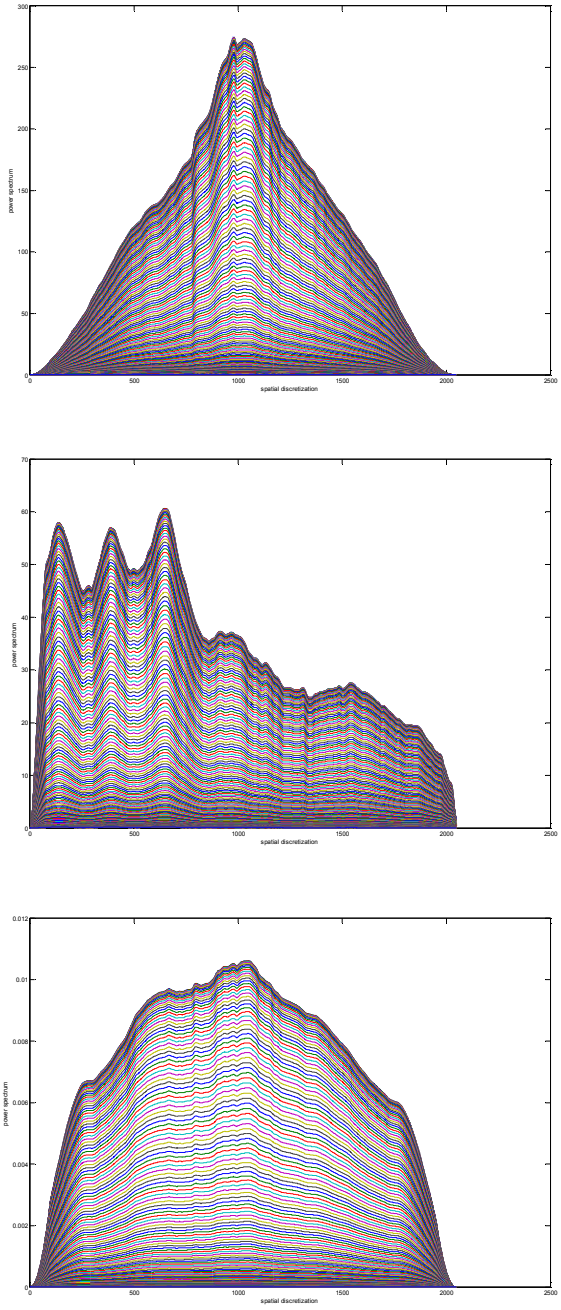

Fig. 4.10 *Evolutionary power spectra of global imperfections u,v and ϑ.*

Chapter 5

COLUMNS BUCKLING ANALYSIS

5.1 Introduction

In order to examine long columns' buckling behavior it is firstly necessary to discretize their perfect geometry with a certain number of finite elements and then enter the imperfections in the nodal coordinates of the perfect shape. The loading and supporting conditions are then entered in the model and the material properties as well. In the present study, the stochastic analysis is referred only to the geometric imperfections and all the other properties of the members are defined deterministically by specific values. The main purpose is to define the level of effectiveness that imperfections have on the buckling loads towards the buckling load of the perfect column.

5.2 Discretization

The cross-sections of the examined columns are considered as thin walled and have the following geometric properties:

B_f=175mm

D=260mm

t_f=t_w=5mm και t_{weld}=5.9mm

L=4000mm

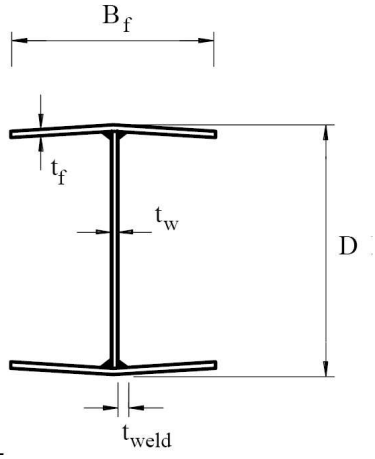

Figure 5.1 *Cross-section geometric properties*

The mesh of the finite elements is designed on the perfect column and consists of three-nodal triangular finite elements with a total of 18 degrees of freedom, which means 6 per node (three displacements and three rotations). The nodal coordinates of the elements are given by Matlab and the imperfections are being entered on them. The discretization of the perfect column is shown in the Fig. 4.2.a. It consists of 250 elements on column's length direction, 12 elements on its width direction and 16 elements on its height direction, as shown in Fig.4.2.b.

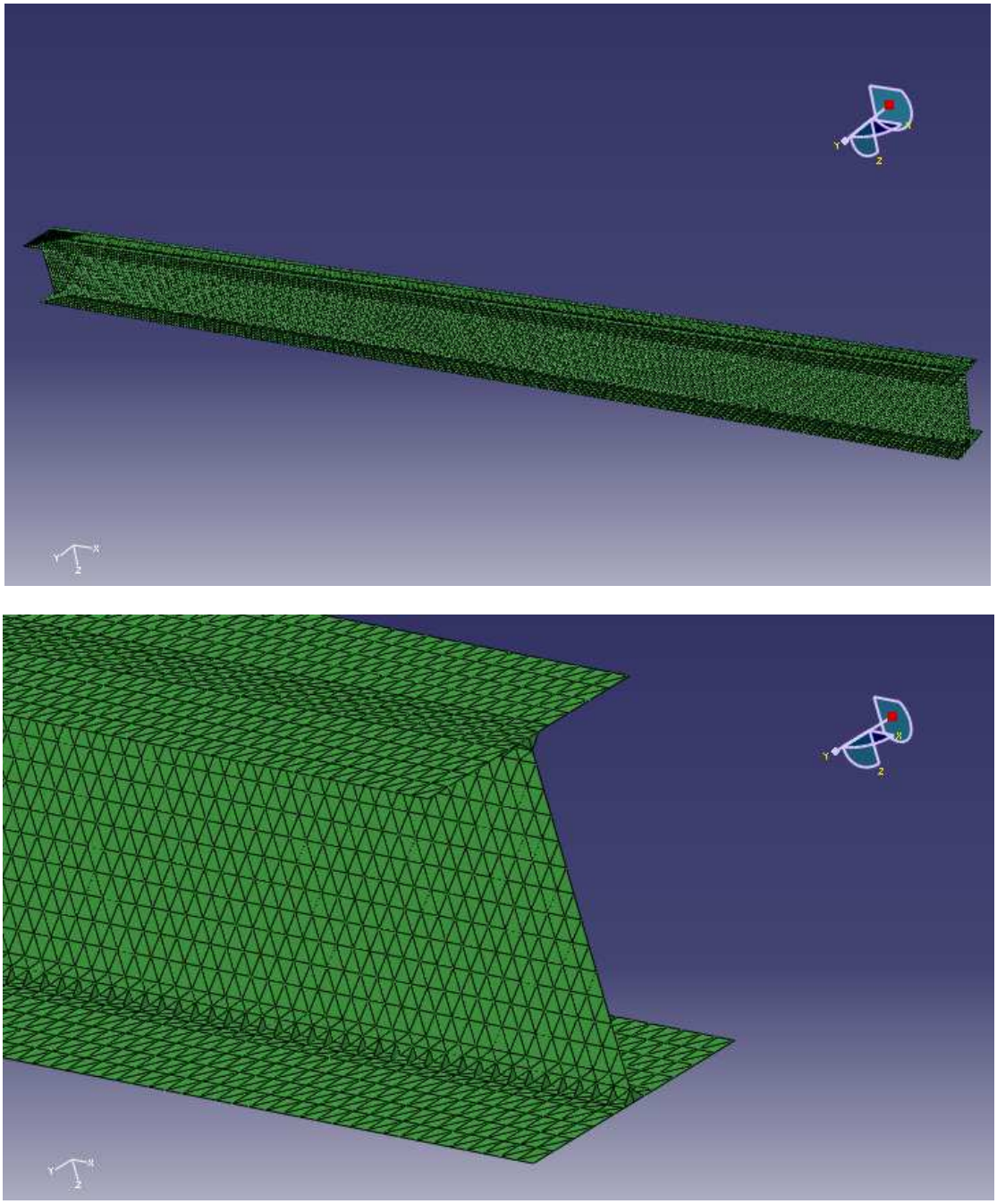

Fig. 5.2 *Column FE discretization*

The web-flange junctions have been also simulated by triangular elements of a smaller side compared to the main elements used for the whole discretization as shown in Fig.4.2.b. The elements that are used have the following dimensions:

- Main flange elements:
  EleL=4000/250=16mm
  EleB=175/10=17.5mm

- Centre flange elements
  EleL=4000/250=16mm
  EleB=(175/10)/2=8.75mm

- Main web elements:
  EleL=4000/250=16mm
  EleB=255/14=18.214mm

- Web-flange junctions:
  EleL=8.75mm
  EleB=9.107mm

According to the above, the model consists of 21000 elements, which corresponds to 10291 nodes and 30873 degrees of freedom.

The thickness of the cross-section and so the thickness of the elements is assumed to be 5mm. Even though there is data available for thickness imperfections, in this study such kinds of imperfections are not being entered in the computations.

5.3 Imperfections

The experimental measurements of the imperfections provided by Hasham and Rasmussen refer to a total number of nine global and local imperfections of the cross-sections, as shown in figure 4.3 (δ_1-δ_9). These measurements have been done on the free edges of the flanges (δ_1,δ_3,δ_5,δ_7), on the centre of the cross-section (δ_4), on web-flange junctions (δ_2,δ_6) and on the outer edges of the flanges (δ_8,δ_9). From δ_2,δ_6,δ_8 and δ_9 we extract the three global imperfections u,v and θ, that refer to the global displacements and the global rotation of the cross-section, while the local imperfections are considered to be the measurements of δ_1, δ_3, δ_4 , δ_5 and δ_7.

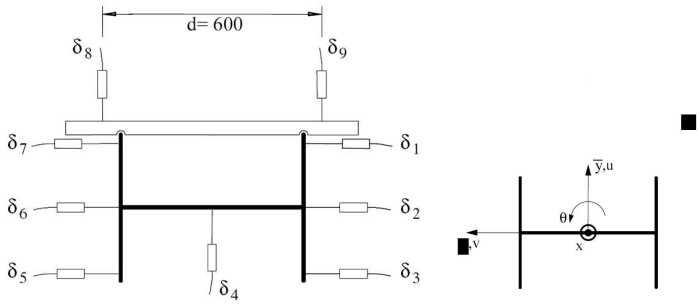

Fig. 5.3 *Local and global imperfections.*

We conclude that from the nine measurements result eight values of imperfections: three global and five local. The global imperfections result as cited:

$$u = \frac{(\delta_8 + \delta_9)}{2}$$
$$v = \frac{(\delta_2 - \delta_6)}{2} \qquad (5.1)$$
$$\vartheta = \frac{(\delta_9 - \delta_8)}{2}$$

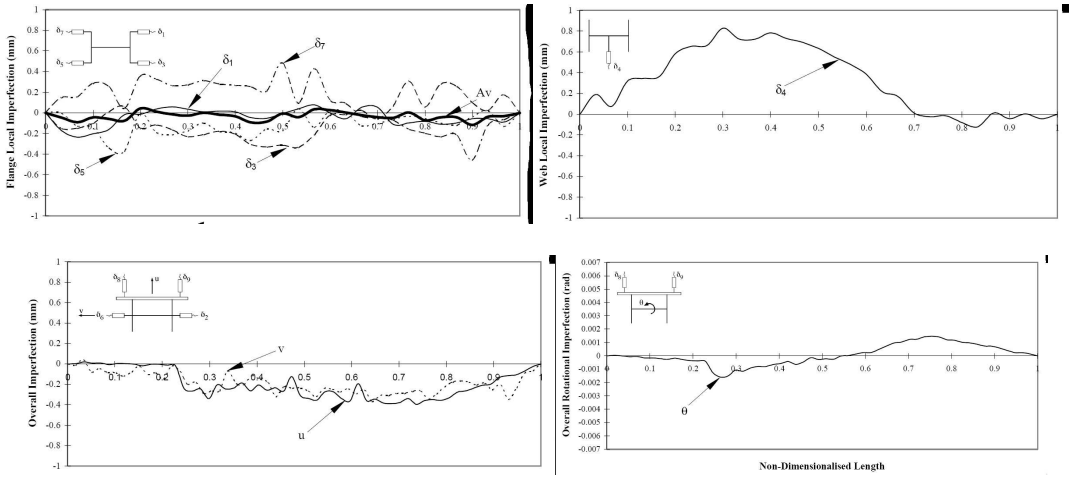

Fig. 5.4 *Imperfection diagrams from Hasham and Rasmussen (1997) measurements.*

It should be noticed that imperfections along the column are neglected. This means that the exact length does not change and imperfections refer to y and z directions and rotations on yz-plane.

There are also available measurements of the other geometric and mechanical properties, such as the thickness, the Young's modulus and the yield stress, that could lead to the assumption that these values could be considered as stochastic procedures. In the present study it is investigated the behavior of a member with stochastic imperfections and so all the other properties of the geometry and the material are defined deterministically, so that:

- Thickness: t=5mm
- Young's modulus: E=210000N/mm^2
- Poisson's ratio: ν=0,3
- Yield stress: σ_y=400N/mm^2

All the above measurements have been made on 2m long beams. The reduction to the 4m long members can be made by scaling the already known power spectra from Schillinger's thesis (2008). Power spectra estimation is of great importance, because then the functions that describe the imperfections of the nodes can be extracted by them and be entered in the FE model.

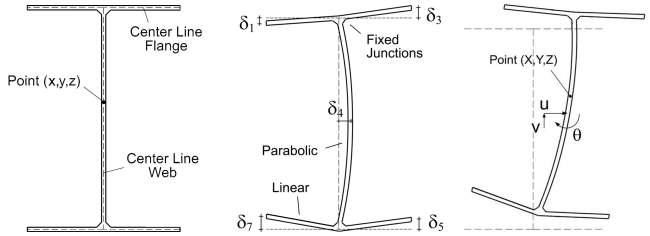

Fig. 5.5 *Mapping from Perfect to Imperfect Geometry.*

The functions of the 8 imperfections according to the spectral representation method are:

$$f^{(i)}(x) = \sqrt{2}\sum_{n=0}^{N-1}\sqrt{2S^{(i)}(\omega_n)\Delta\omega}\cos(\omega_n x + \varphi_n) \qquad (5.2)$$

$where:$

$n = 0,1,...,N-1$

$i = 1,2,...,8$

The devolvement from perfect to imperfect geometry is done by the following procedure. The affection of global imperfections u, v and θ on the perfect geometry is:

$$\begin{bmatrix}\Delta Y_{glob}\\ \Delta Z_{glob}\end{bmatrix}(x,y,z) = \begin{bmatrix}U\\ V\end{bmatrix}(x) + \begin{bmatrix}f_u\\ f_v\end{bmatrix}(x) + \begin{bmatrix}\cos(\Theta+f_\theta) & -\sin(\Theta+f_\theta)\\ \sin(\Theta+f_\theta) & \cos(\Theta+f_\theta)\end{bmatrix}(x)\cdot\begin{bmatrix}y\\ z\end{bmatrix} \qquad (5.3)$$

Where:

(x,y,z) → perfect geometry

(X,Y,Z) → imperfect geometry

x=X

$f_u(x) = f_6(x)$

$f_v(x) = f_7(x)$

$f_\theta(x) = f_8(x)$

U(x),V(x),Θ(x) → mean values of global imperfections.

The above equation expresses the distortion of the nodal coordinates from the perfect shape. So, the final geometry and coordinates are:

$$\begin{bmatrix} Y \\ Z \end{bmatrix}(x,y,z) = \begin{bmatrix} y \\ z \end{bmatrix} + \begin{bmatrix} \Delta Y_{glob} \\ \Delta Z_{glob} \end{bmatrix}(x,y,z) + \begin{bmatrix} 0 \\ \Delta Z_{f\lg,i}(x)\dfrac{y_i}{w} \end{bmatrix} + \begin{bmatrix} \Delta Y_{web}(x)\left(1-\dfrac{z_i^2}{H}\right) \\ 0 \end{bmatrix} \qquad (5.4)$$

Where:
W=87.50mm
H=127.50mm

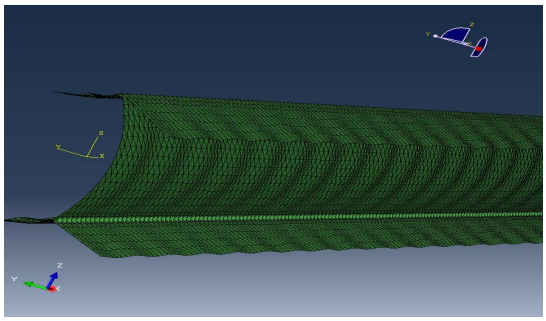

Fig. 5.6 *Complete Imperfect Geometry. All local imperfections have been scaled by factor lambda=300.*

5.4 Boundary and Loading Conditions

The 4m long columns examined in this chapter are analyzed in compression according to two different boundary conditions. In the first case, all degrees of freedom of the left edge are constrained and in the second case the left edge is also tied and the middle node of the right edge is pinned. Furthermore, the displacements of the nodes of the right edge in both cases are related to the displacements of the middle node, where the loading is being applied on.

The loading at both cases is being applied on the right edge of the column as a concentrated force at the middle node of the I cross-section, which is the reference point. Using the ABAQUS, all the degrees of freedom of the nodes of the right edge have been related to the reference point. This means that the edge moves as a rigid body according to the displacements of the reference point.

This assumption describes better the real behavior of the structure than the distributed loads at the nodes of the right edge, because they affect locally the behavior of the structure.

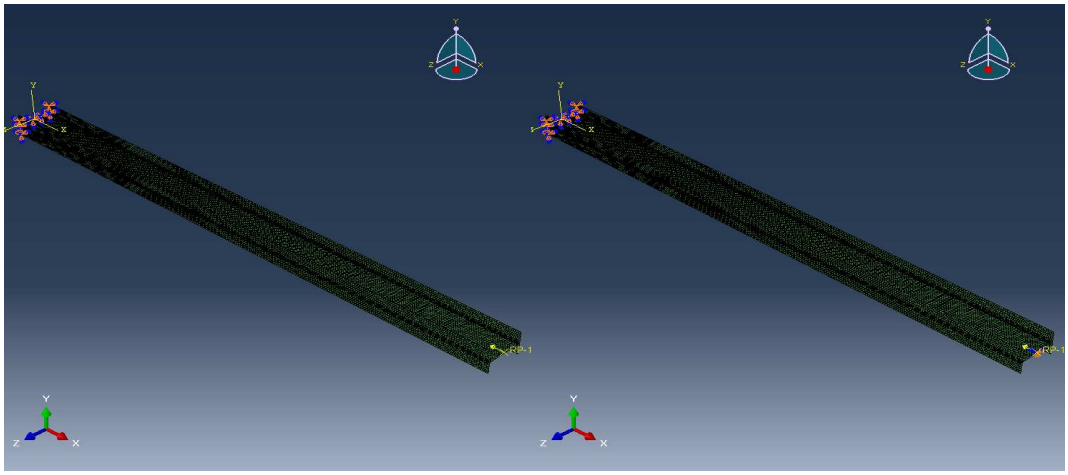

(a) *(b)*

Fig. 5.7 *Boundary and Loading Conditions at both cases (a) one edge completely tied and (b) one edge tied and the other one pinned .*

The initial compressive loads are $P_{in,a}$=200kN and $P_{in,b}$=1500kN.

5.5 Results

For the present chapter, 50 columns with random imperfections have been studied under axial compression in order to extract a stochastic evaluation of the critical buckling load. Here are presented the results for both boundary conditions.

(a) Cantilever Columns

At first the perfect column is being submitted in eigenvalue analysis in order to obtain the critical buckling load. It has been proved that the critical buckling load can be computed if the first eigenvalue (λ_1) and the initial loading (P_{in}) are known, as follows:

$$P_{cr,eigen} = \lambda_1 \cdot P_{in} \qquad (5.5)$$

In Fig. 5.8 are presented the first three eigenmodes and eigenvalues. It can be easily concluded that the first eigenmode describes the phenomenon of global buckling, with critical buckling load $P_{cr,eigen}$=149.08 kN, according to Eq. (5.5). The second eigenmode describes the torsional and the third the local buckling.

It has also been calculated the Euler critical buckling load, as:

$$P_{cr,Euler} = \frac{\pi^2 EI}{(2L)^2} \qquad (5.6)$$

that leads to: $P_{cr,Euler}$ = 144.72 kN

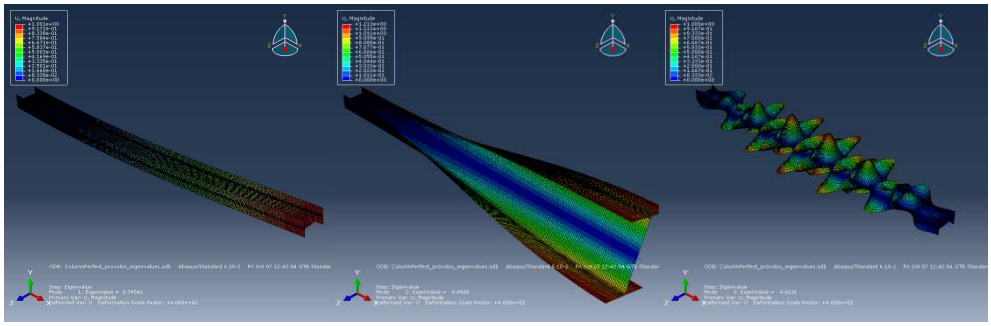

(α) λ_1=0.74542 *(b) λ_2=4.4569* *(c) λ_3=4.8131*

Fig. 5.8 *Three first eigenmodes and eigenvalues of the perfect column.*

The next step is to estimate the critical buckling load of the perfect column from the nonlinear analysis of it in axial compression. In Fig. 5.9 it is shown the force-displacement diagram and the deformed shape. The critical buckling load from the nonlinear analysis is $P_{cr,perf}$ = 149.19 kN.

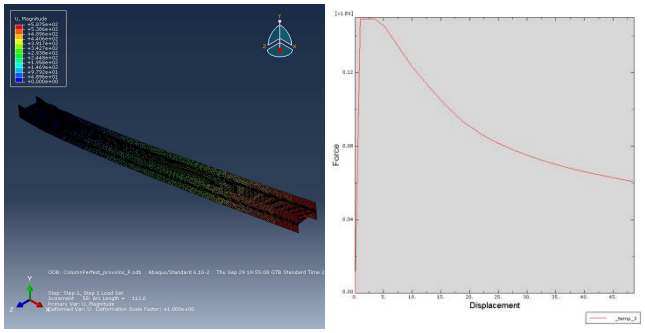

Fig. 5.9 *Force-displacement diagram and deformed shape of the perfect column under axial compression.*

The same analysis has been applied on the sample of the 50 imperfect columns. In Fig. 5.10 it is shown the deformed shape and the force-displacement diagram of a random imperfect column. In Fig.5.11 it is shown a histogram of the stochastic critical buckling loads in Table 5.1 it is shown a comparison between the theoretical and the mean values.

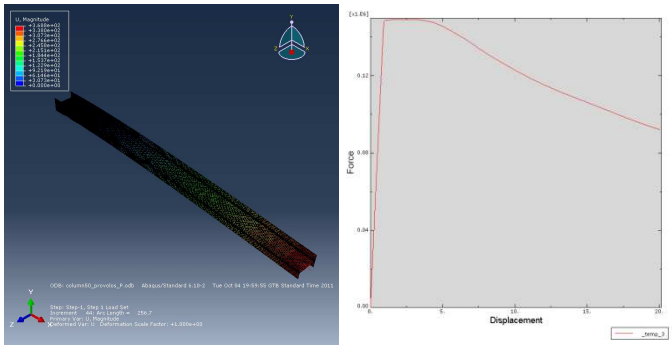

Fig. 5.10 *Force-displacement diagram and deformed shape of a random imperfect column under axial compression.*

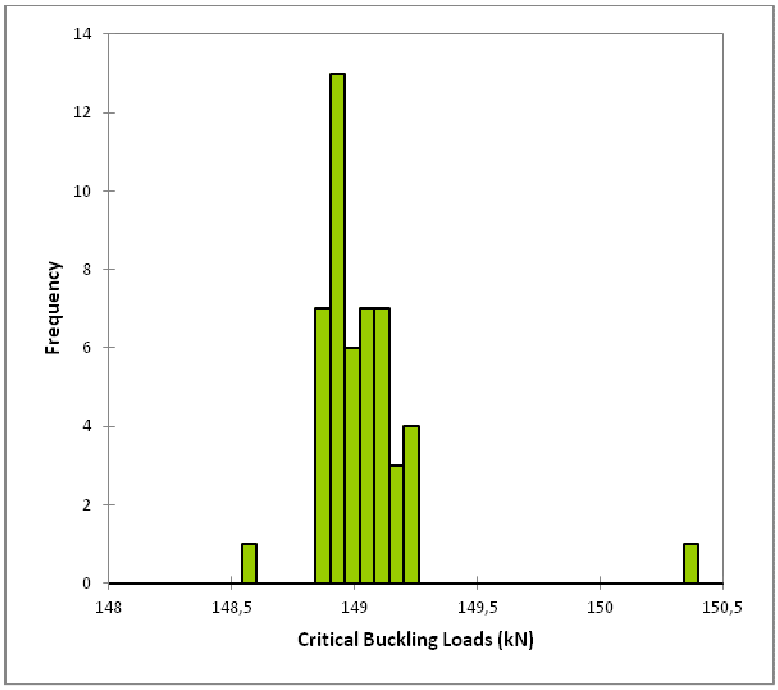

Fig. 5.11 *Histogram of the stochastic critical buckling loads of cantilever columns.*

According to Fig.5.11 the statistical properties of the sample of the stochastic analysis are the following:

$P_{cr,mean}$=149.05 kN

StDev=0.23 kN

CoV=0.15%

	Euler	Eigenvalue Analysis	Perfect Column	Mean value from the stochastic analysis
Critical buckling load (kN)	144.72	149.08	149.19	149.05

Tab. 5.1 *Comparison of the critical buckling loads.*

From the results presented above it can be easily concluded that in cantilever columns the influence of the imperfections is almost zero. It can be seen that the reduction of the strength is about 0.1%. All the columns of the sample are lead to global buckling. It can be observed from the statistical results that the influence of geometric imperfections in cantilever beams-columns is practical zero. All columns fail according to the first eigenmode, which is the mode that describes the global buckling failure. In opposition to short length members, imperfections do not activate any other mode of failure, except from the first one. It can be easily concluded from the really small values of the coefficient of variance which in our

case is 0.15% and in short long columns is about 2%, while in cylindrical shells under axial compression is between 6 and 8% (Papadopoulos and Papadrakakis 2005).

(b) Tied-pinned Columns

The same procedure as described above has been followed on the stochastic analysis of tied-pinned columns. The boundary conditions described below are shown in Fig. 5.12 as well as the initial loading $P_{in,b}$=1500kN and the first eigenmode.

Edge 1: U1=U2=U3=UR1=UR2=UR3=0

Edge 2: U2=U3=UR1=UR3=0

This means that the left edge of the column is completely tied in all directions and the right one is pinned on the y-dimension. Rotations around the y axis are unconstrained and displacement along the longitudinal axis x. The force is also compressive with direction along the negative values of x-axis.

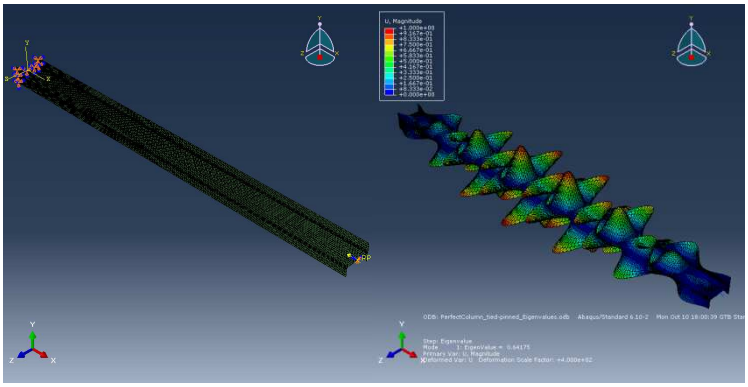

Fig. 5.21 *Boundary Conditions and 1st eigenmode.*

The first eigenmode, with eigenvalue λ_1=0.64175, describes the local buckling phenomenon. The critical buckling loads are shown in Tab. 5.2. In Fig.5.22 is shown the typical deformed shape of vast majority of the columns examined in this section, as well as the force-displacement diagram.

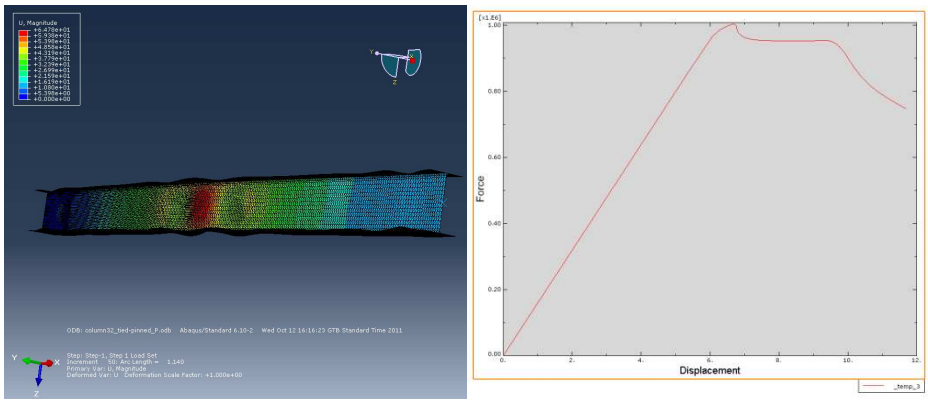

Fig. 5.22 *Deformed Shape of a random imperfect column and force-displacement diagram.*

In Fig.5.23 is shown the histogram of the stochastic critical buckling loads of tied-pinned columns. As we can see, the vast majority of the resulting loads are between 999 and 1016 kN and only a few of them have much greater values, closer to the critical buckling load of the perfect structure and the Euler critical buckling load, while the load resulting from the first eigenmode is much lower.

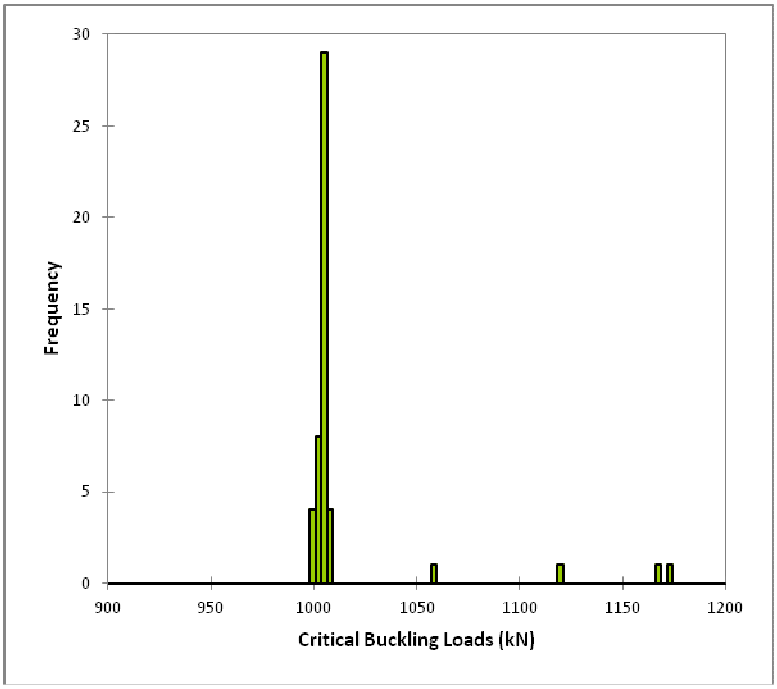

Fig. 5.23 *Histogram of the stochastic critical buckling loads of tied-pinned columns.*

	Euler	Eigenvalue Analysis	Perfect Column	Mean value from the stochastic analysis
Critical buckling load (kN)	1181.38	962.63	1205.75	1014.24

Tab. 5.2 *Comparison of the critical buckling loads of tied-pinned columns.*

The values of the first four classes of the histogram shown in Fig. 5.23 are really close to the critical load resulting from the 7^{th} eigenvalue, which is λ_7=0.67395 and leads to a load of $P_{cd,eigen,7}$=1010.93 kN, while the values of the last two classes are close to the load resulting from the 16^{th} eigenvalue λ_{16}=0,79041 which leads to $P_{cr,eigen,16}$=1185.62 kN, that is also close to the Euler critical buckling load. It can be concluded that in tied-pinned columns under axial compression the mechanism of failure consists of local buckling according to the 7^{th} eigenmode. According to eigenvalue analysis of the perfect column, the 5^{th} and the 6^{th} non-zero classes follow the equilibrium path of the 11^{th} and 13^{th} eigenmode.

The statistical properties of the sample are the following:

$P_{cr,mean}$=1014.24 kN

StDev=37.43 kN

CoV=3.69%

From the value of the coefficient of variance it can be concluded that the scattering of the buckling loads of tied-pinned columns is much bigger than cantilever columns. This also indicates that imperfections have a great impact on the value of the buckling load in this kind of columns. The reduction of the column strength results to be about 19%. This means that not only imperfections but also boundary conditions of an imperfect member play an important role on its total strength and the scattering of the buckling loads.

Chapter 6

FRAMES BUCKLING ANALYSIS

6.1 Introduction

This chapter examines the buckling behavior of imperfect frames, through the variation of the critical load of instability according to the members' imperfections. In order to avoid instability of the frames because of a beam-column junction failure, they have been properly reinforced. There have been used the imperfections data that of the previous chapter that has to do with columns buckling analysis. The junctions are supposed to be perfect, which means that their shape is perfect, videlicet in the nodal coordinates of the junctions no imperfections are entered, as is done in the other nodes of the frame.

6.2 Discretization

The discretization of the frames is the same as the one of the columns with the difference that there are some elements added in the beam-columns junctions. The frames consist of a total of 33723 nodes, 69268 elements and 202338 degrees of freedom, see Fig. 5.1.

The members of the frame have the same geometric properties with the columns examined in the previous chapter. The difference is that in order to use the same geometry in the members it was necessary to add some elements in the beam-column junctions, so that it would not be needed to change the discretization of the members. The junctions added in order to create the frame have H=255mm height and B=175mm width, as shown in the Fig. 5.2. Apart from that, six flanges have also been added in order to reinforce the junctions and prevent their failure, before the collapse of the frame itself. Adding these flanges the junctions' shape becomes cubical.

According to the above the total length of the frame becomes L+H+H=4510mm, the total height L+H=4255mm and width B=175mm, see Fig. 5.3.

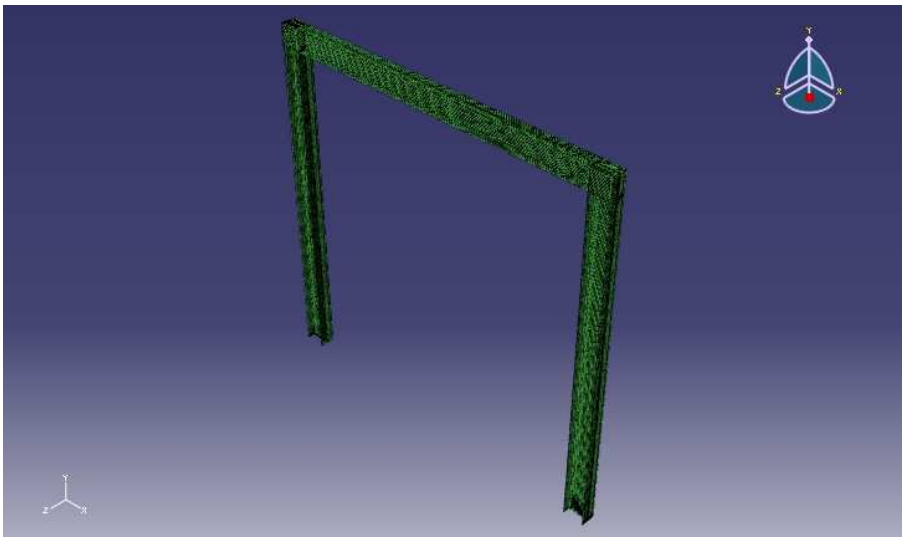

Fig.6.1 *Discretization of the frame.*

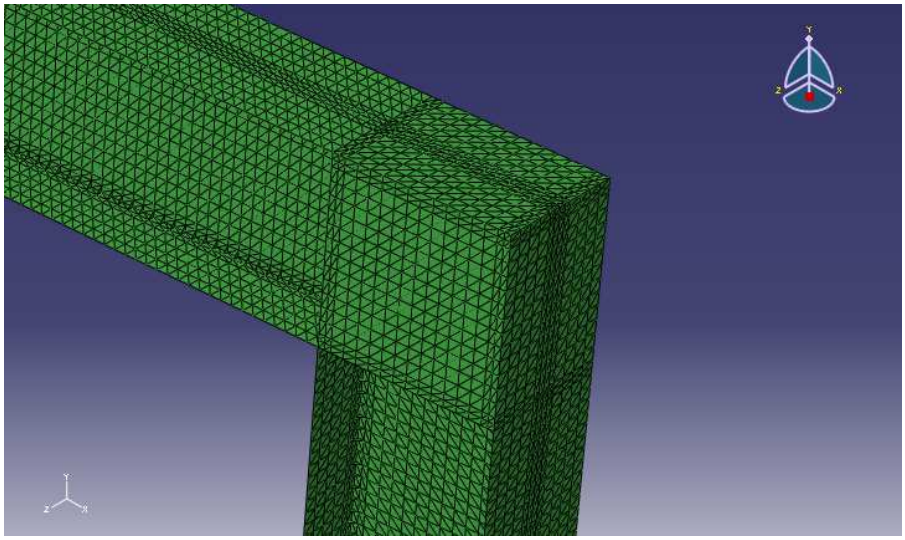

Fig. 6.2. *Discretization of the beam-column junction.*

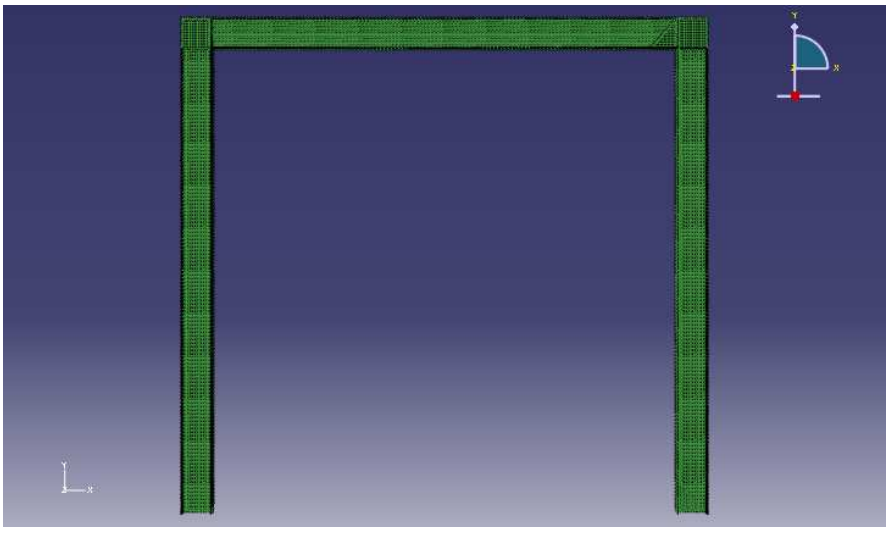

Fig. 6.3. *Frame geometry.*

6.3 Imperfections

The imperfections of the members are the same as these used in the 4 meters long columns examined in the previous chapter. The beam-column junctions are supposed to be perfect, so the extra nodes that have been added have no imperfections. So, it is assumed that the imperfections do not take at the end of the members and the beam-column junctions' shape is perfect.

It is also assumed that the imperfections of the three members of the frame are not the same. This means that a different set of imperfections is used per member. This assumption helps as to be more accurate on our computations and indicates the stochastic nature of the imperfections of a real structure. This also means that the imperfections of the members are independent from each other.

It should be noted that the imperfections included in the imperfect geometry of the frame have nothing to do with those referred to the Eurocode 3 about imperfections for global analysis of frames. The EC3 takes under consideration the global imperfections by an initial sway imperfection of the whole frame (ϕ) and individual bow imperfections of the members separately and the local imperfections of members for flexural torsion by a relative initial local bow imperfection (e_0). Global imperfections may be disregarded when $H_{ED} > 0.15V_{ED}$ and local imperfections should be accounted for in a member when $N_{ED} > 0.25N_{cr}$.

6.4 Boundary Conditions

All degrees of freedom of the nodes at both ends of the frame have been completely constrained. The other nodes are unconstrained, which means that the frame can deform in all directions. It can be led to an out of plane deformation; videlicet the frame is gone through a full 3D non linear analysis.

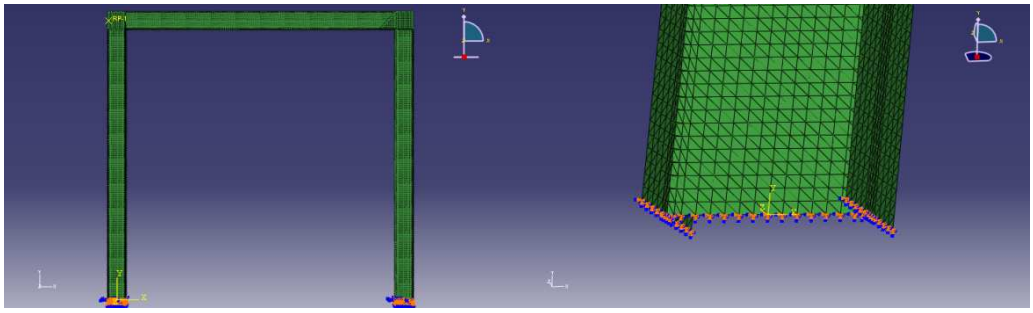

Fig. 6.4. *Fully constrained boundary conditions (a) at both ends of the frame and (b) zoom at the first end of the frame.*

Degrees of freedom that have been constrained are, analytically:

- U1=0 → transform along x-axis.
- U2=0 → transform along y-axis.
- U3=0 → transform along z-axis.
- UR1=0 → rotation about x-axis.
- UR2=0 → rotation about y-axis.
- UR3=0 → rotation about z-axis.

6.5 Loading

A horizontal and a vertical load are supposed to be acting on the structure. These loadings have been equally contributed on the nodes of the frame that they act and correspond to the initial loads that are used by the Arc Length Method in order to define the critical buckling load of the frame. The loads have been equally distributed to the nodes that they act and the horizontal corresponds to 1000 Newton per node and the vertical 12.5 Newton per node, see Fig. 5.6 and Fig. 5.7.

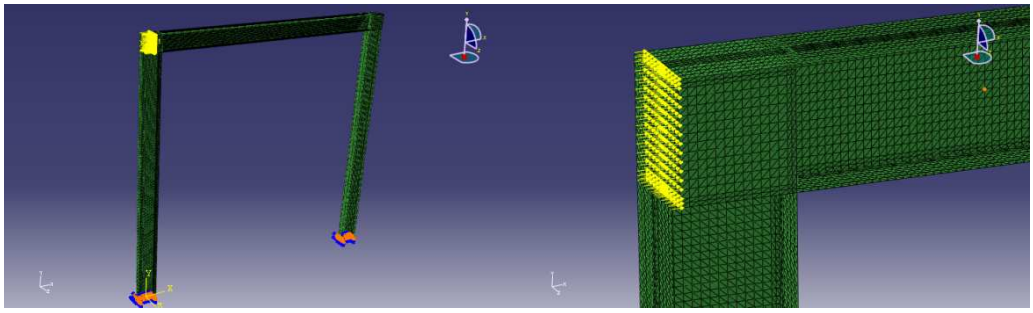

Fig. 6.6. *Horizontal loading distributed on the nodes of the right beam-column junction.*

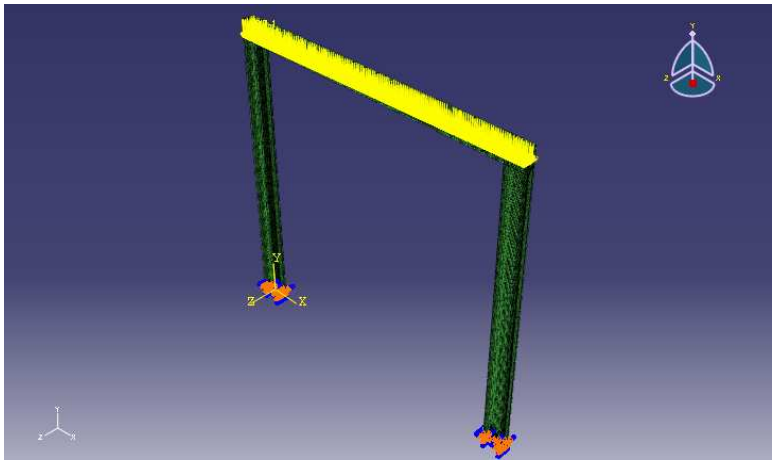

Fig. 6.7. *Vertical loading distributed on the nodes of the upper flanges of the beam and the beam-column junctions.*

6.6 Results

Main purpose of this chapter is to extract the stochastic critical buckling loads of an imperfect frame using the Monte Carlo Simulation. There have been examined 100 sets of imperfections, which means that there have been extracted 100 critical buckling loads by 100 different imperfect frames.

At first we obtain the Force-Displacement diagram of the structure on a specified reference point, see Fig. 6.8. According to Fig. 6.8 the critical buckling load of a frame is about 450N/node. The displacement increases with the force until the structure becomes unstable.

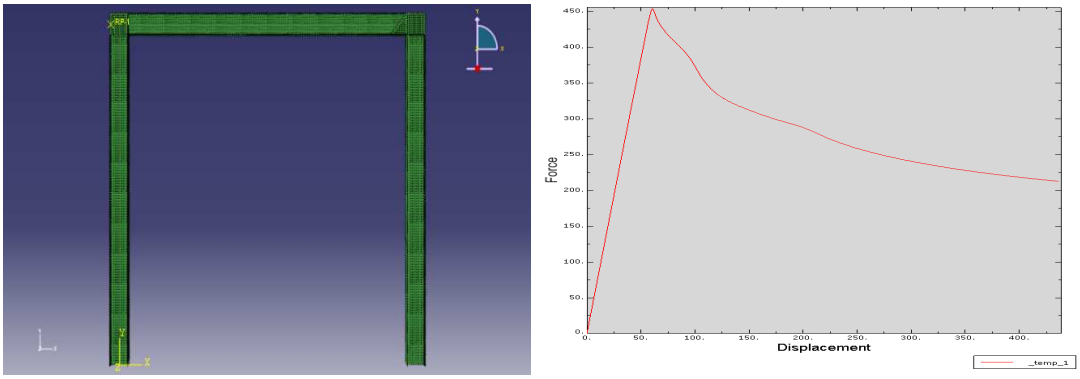

Fig. 6.8 *Reference Point of the Frame and force-displacement diagram.*

In Fig.6.9 is shown the deformed shape of the frame. When the force increases the right column fails in buckling and then the frame becomes instable and rotates around the y-axis.

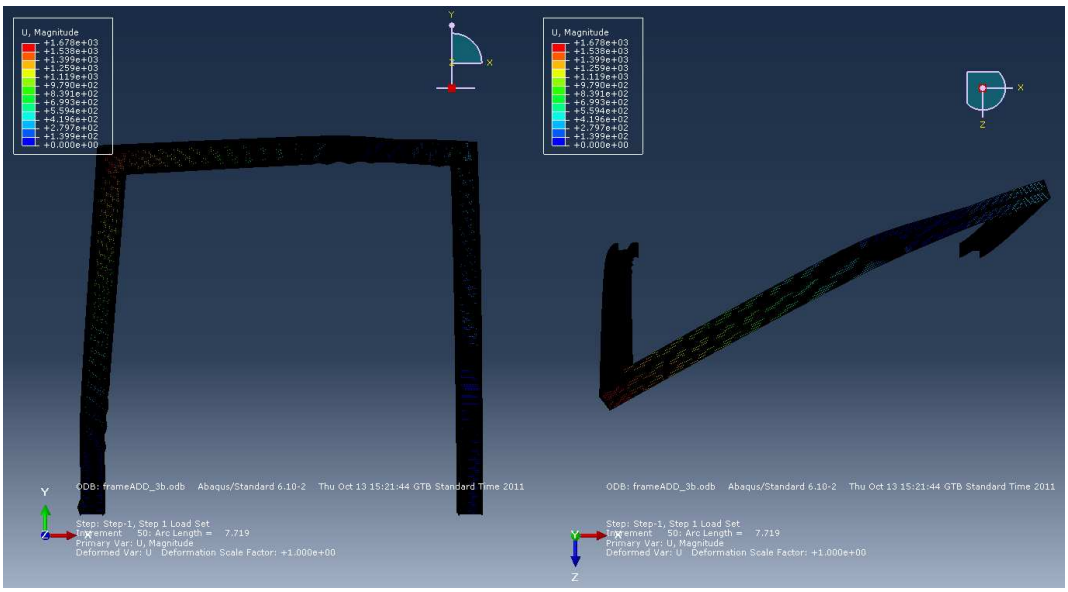

Fig. 6.9 *Deformed Shape of a random imperfect frame.*

In Tab.6.1 are shown the critical buckling loads of the perfect and imperfect frames (mean value). Comparing these values we see a reduction of the strength of the frame about 40%. This means that initial geometric imperfections have an impact of great importance on the total strength of frames. It should be noted here that initial angle imperfections of the frame, that are being cited as global imperfections in Eurocode 3, have been neglected. The most likely is that taking these extra imperfections under consideration, the reduction of the total strength becomes much bigger.

In Fig. 6.10 is shown the histogram of the stochastic critical buckling loads. The statistical results are the following:

$P_{cr,mean}$=101.51 kN

StDev=6.34 kN

CoV=6.24%

The big value of the coefficient of variance indicates the important role of the initial imperfections in the variation of the critical buckling load.

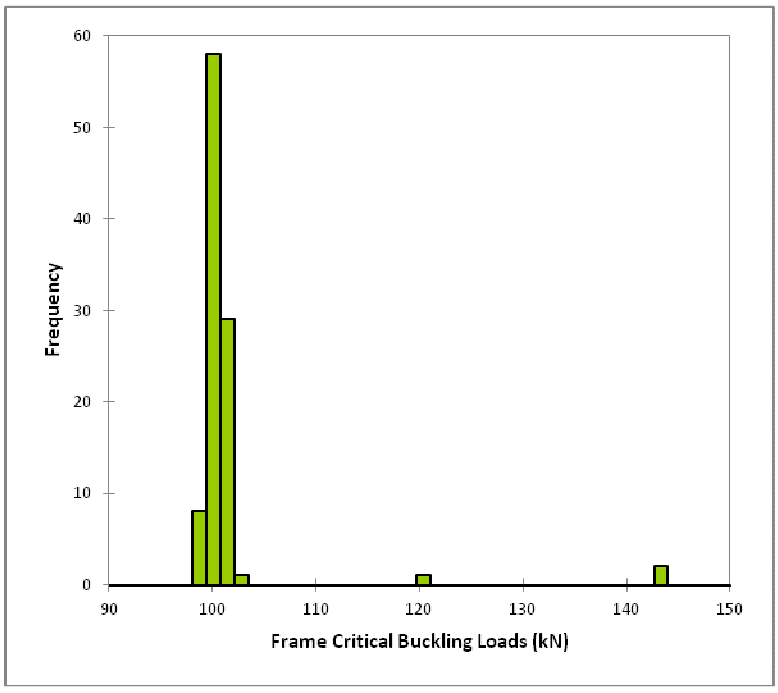

Fig. 6.10 *Histogram of the stochastic critical buckling loads of imperfect frames.*

	Perfect Frame	*Imperfect Frames (Mean Value)*
Critical Buckling Load (kN)	*142.08*	*101.51*

Tab. 6.1 *Critical buckling loads.*

The characteristic scattering of the buckling loads is much bigger than imperfect columns under axial compression. In the previous chapter it has been calculated the value of coefficient of variance for tied-pinned columns as 3.69%, while in two meters columns it is about 2% (Schilliger 2008). So, the dubiety in determining the exact buckling load of frames is proven to be much more difficult and complicated than in single members, such as beams and columns. Local imperfections seem to have a greater impact on the ultimate strength of frames. This means that common steel structures – whose beams-columns junctions react like frames – need to be very carefully designed. The reduction of the total strength is much greater too from single members. This means that global non-linear analysis approaches much better the real behavior than any other method proposed in EC 3.

Chapter 7

CONCLUSIONS AND FUTURE PROSPECTS

7.1 Conclusions of Accomplished Work

Main target of this work was to examine the buckling behavior of long length geometrically imperfect columns and frames by use of random process theory and advanced finite element methods. Imperfections generally reduce the ultimate strength of structures. By assuming that they can be expressed as stochastic random fields – Gaussian random fields – it is easier to define the level of scattering of the resulting critical buckling load. So, it was of great importance the correct and accurate modeling of the perfect, at first, and the imperfect geometry of the structures by entering the functions that imply the global and local imperfections.

By using the power spectra for 4m long columns, calculated by Schillinger D., it was easy to define the functions of imperfections with the spectral representation method. The values of these functions indicate the distortion of the nodes of the FE mesh from the perfect shape. After the definition of the imperfect geometry of the nodes of the columns, it was necessary to define the connectivity matrix – the matrix that defines the nodes of every single triangular shell element – for the Abaqus input file, as well as the material properties and the loading and boundary conditions.

There have been examined 4m long columns with two different types of boundary conditions (cantilever and tied-pinned columns), in order to study the influence of imperfections in buckling analysis. In frames, there have been used 4m long members with different sets of imperfections. In addition, the beam-column junctions have been reinforced with extra steel plates in all directions, so there shape would become cubical, in order to avoid its failure under any type of loading.

After that, there have been made 50 Monte Carlo Simulations for the two different types of beam-columns under axial compression and 100 for frames, from which the stochastic critical buckling load was extracted.

For the cantilever columns it has been clear that the influence of imperfection on the critical buckling load is almost zero. All simulated columns failed for the same axial load as the perfect-shaped one, which refers to the first eigenmode, videlicet all columns failed by global buckling.

For the tied-pinned columns, the scattering of the resulting buckling load was much higher than the cantilever ones and the coefficient of variance was about

3.7%. This indicated the influence of the boundary conditions in axial compression. Also, the vast majority of the simulated columns failed by local buckling, while the ultimate compression strength of imperfect columns was reduced about 20%, compared to the total strength of the perfect one.

For the frames, it has been observed a reduction of the total strength about 40%, while the characteristic scattering of the critical load has proven to a little smaller than 7%. This indicates the important role of initial geometric imperfections in frames stability analysis. It can also be concluded that imperfections affect more the global stability of framed structure than the ultimate buckling strength of a single member. Frame structures are proven to be more sensitive in initial imperfections than any other kind of single member.

7.2 Future Prospects

In this work have been examined 4m long imperfect columns under axial compression. Future research can be conducted in order to extract the stochastic interactive curve, which means that columns should be tested under combined compression and major axis bending. Also, more research is needed in order to examine the scattering of the resulting critical loads in proportion to the magnitude of imperfections. This means that a parametric analysis on imperfections would give very interesting results. A stochastic approach of thickness imperfections and other material properties, such as the Young's modulus, the Poisson's ratio and residual stresses that in this work have been defined deterministically or neglected at all, would describe much better the real behavior of thin-walled beam-columns.

In frames buckling analysis of the present study, the biggest witting omission is the luck of angle imperfections, which are in EC 3 cited as global imperfections. So, more research is available by adding this kind of imperfections, as well as changing the boundary conditions and the magnitude of imperfections.

Apart from that, no research has been made for steel truss systems, which are widely used in construction industry. Furthermore, boundary imperfections seem to be a great challenge for every researcher.

As far for the used methodology, there is much space to work on techniques that would reduce the large computational demand of the Monte Carlo Simulations. That was also a problem that occurred during the research of the present study, because of the high number of DOFs, especially in frames buckling analysis.

Another topic that would improve the accuracy of the results is the expression of imperfections as non-Gaussian random fields. This would lead in a more realistic modeling of the imperfect shape and so better results could be conducted.

At last, it would be of great importance the existence of data for measured imperfections for long columns, with also experimental tests under different kinds of loading. Then the results of the simulations could be compared to the results of the experiments. This would be very helpful in order to check the reliability of the simulations.

Chapter 8

BIBLIOGRAPHY

8.1 English Bibliography

Argyris, J.H., Papadrakakis, M., and Stefanou G. (2002). *"Stochastic finite element analysis of shells"*, Comp. Meth. Appl. Mech. Engrg. 191, 4781-4808.

Argyris, J.H., Papadrakakis, M., and Karapitta, L. (2002). *"Elastoplastic analysis of shells with the triangular element TRIC"*, Comp. Meth. Appl. Mech. Engrg. 191(3), 3613-3637

Bathe, K.J. (1996). *Finite Element Procedures*, Prentice Hall, Upper Saddle River, NJ.

Becque, J., and Rasmussen, K.J.R., (2007). *Experimental investigation of the Interaction of Local and Overall Buckling of Stainless Steel I-Columns*, Research Report No R887, School of Civil Engineering, University of Sydney.

Cohen, L. (1995*). Time-Frequency Analysis*, Prentice Hall, New Jersey.

Deodatis, G. and Shinozuka, M. (1988). *"Auto-Regressive Model for Non-Stationary Stochastic Processes"*, J. Eng. Mech., ASCE, 114(11), 1995-2012.

Fishman, G. (2001). *Monte Carlo: Concepts, Algorithms and Applications*, Springer, New York.

Greiner, R., Kettler, M., Lechner, A., Freytag, B., Linder, J., Jaspart, J.P., Boissanade, N., Bortolotti, E., Weynand, K., Ziller, C., and Oerder, R. (2008b). *Plastic Member Capacity of Semi-Compact Steel Sections – a more Economic Design*, Final Report, SEMI-COMP: RFSR-CT-2004-00044, European Research Fund for Coal and Steel.

Hasham, A.S. and Rasmussen, K.J.R., (1997). *Member Capacity of Thin-Walled I-sections in Combined Compression and Major Axis Bending*, Research Report No R746, School of Civil Engineering, University of Sydney.

Hasham, A.S. and Rasmussen, K.J.R., (2001). *"Nonlinear Analysis of Locally Buckled I-section Steel Beam-Columns"*, in Zaras J,. Kowal-Michalska K., and Rhodes J. (Eds.), Thin-Walled Structures – Advances and Developments, Proc. 3rd Int. Conf. on Thin-Walled Structures, Krakow, 427-436, Elsevier.

Hasham, A.S. and Rasmussen, K.J.R., (2002*). "Interaction curves for locally buckled I-section beam-columns"*, J. of Constructional Steel Research 58, 213-241.

Kala, Z. (2005). *"Sensitivity analysis of the stability problems of thin-walled structures"*, J. of Constructional Steel Research 61, 415-422.

Mallat, S. (1999). *A Wavelet Tour of Signal Processing*, Academic Press, New York.

MatLab (2009). *MatLab user's guide*, MathWorks Inc., Natick, MA.

Landau, P.D., and Binder, K. (2005). *A Guide to Monte Carlo Simulations in Statistical Physics*, Cambridge University Press, UK.

Newland, D.E. (1993). *An Introduction to Random Vibrations, Spectral and Wavelet Analysis*, Longman Scientific & Technical, London.

Okazawa, S., Oide, K., Ikeda, K., and Terada, K. (2002). *"Imperfection sensitivity and probabilistic variation on tensile strength of steel members"*, Int. J. of Solids and Structures 39, 1651-1671.

Papadopoulos, V., and Papadrakakis, M. (2004). *"Finite element analysis of cylindrical panels with random initial imperfections"*, J. Engrg Mech., ASCE, 130(8), 867-876.

Papadopoulos, V., and Papadrakakis, M. (2005). *"The effect of material and thickness variability on the buckling load of shells with random initial imperfections"*, Comp. Meth. Appl. Mech. Engrg. 194, 1405-1426.

Papadopoulos, V., and Papadrakakis, M. (2008). *Random Vibrations Theory, Lecture Notes*, Institute of Structural Analysis and Seismic Research, National Technical University of Athens.

Papadopoulos, V., and Iglesis, P. (2007). *"The effect of non-uniformly axial loading on the buckling behavior of shells with random imperfections"*, Int. J. of Solids and Structures 44, 6299-6317.

Papoulis, A. (1990). *Probability and Statistics*, Prentice-Hall, NJ.

Papoulis, A., and Pilai, S.U. (2001). *Probalitity, Random Variables and Stochastic Processes*, McGraw- Hill, New York.

Rasmussen, K.J.R., and Hancock, G.J. (1998). *"Buckling analysis of thin-walled structures: analytical developments and applications"*. Prog. Struct. Engng Mater. 1(3), 316-322.

Rasmussen, K.J.R., and Hancock, G.J. (2000). *"Buckling analysis of thin-walled structures: numerical developments and applications"*. Prog. Struct. Engng Mater. 2(3), 359-368.

Reddy, J.N. (2006). *An Introduction to the Finite Element Method*, third edition, McGraw-Hill, New York.

Schafer, B.W., Grigoriu, M., and Pekoz, T. (1998). *"A probabilistic examination of the ultimate strength of cold-formed steel elements"*, Thin-Walled Structures 31, 271-288.

Schenk, C.A., and Schueller, G.I. (2003). *"Buckling analysis of cylindrical shells with random geometric imperfections"*, Int. J. Non-Linear Mech. 38, 1119-1132.

Schillinger, D. (2008). *Stochastic FEM Based Stability Analysis of I-Sections With Random Imperfections, Diploma Thesis*, University of Stuttgart.

Schillinger, D. and Papadopoulos, V. (2009). *"Accurate estimation of evolutionary power spectra for strongly narrow-band random fields"*, Comp. Methods Appl. Mech. Engrg.

Schillinger, D., Papadopoulos, V., Bischoff, M., and Papadrakakis, M. *"Buckling Analysis of Imperfect I-Section Beam-Columns with Stochastic Shell Finite Elements"*, J. Computational Mechanics, Vol.46, No. 3.

Schillinger, D., and Malla, R.B. (2008). *"Analytical Elastic Solution Based on Fourier Series for a Confined Granular Column"*, J. Engrg. Mech., ASCE 134(11), 937-951.

Shinozuka, M., and Jan, C.M. (1972). *"Digital simulation of random processes and its applications"*, J. Sound Vib. 25, 111-128.

Shinozuka, M., and Deodatis, G. (1991). *"Simulation of stochastic processes by spectral representation"*, Appl. Mech. Rev., ASME 44, 191-203.

Shinozuka, M., and Deodatis, G. (1996). *"Simulation of multi-dimensional Gaussian stochastic fields by spectral representation"*, *"*, Appl. Mech. Rev., ASME 49, 29-53.

Stefanou, G. and Papadrakakis, M. (2004). *"Stochastic finite element analysis of shells with combined random material and geometric properties"*, Comput. Meth. Appl. Mech. Engrg. 193, 139-160.

Timoshenko, S.P., and Goodier, J.N. (1970). *Theory of elasticity*, McGraw-Hill, New York.

Vanmarcke, E. (1983). *Random Fields: Analysis and Synthesis*, The MIT Press, Cambridge, MA.

8.2 Greek Bibliography

Βάγιας, Ι. (2003). *Μεταλλικές Κατασκευές Ανάλυση και Διαστασιολόγηση*, Εκδόσεις Κλειδάριθμος, Αθήνα.

Βάγιας, Ι., Ερμόπουλος, Ι., Ιωαννίδης, Γ. (2005). *Σχεδιασμός Δομικών Έργων από Χάλυβα*, Εκδόσεις Κλειδάριθμος, Αθήνα.

Ματαράς, Δ.Σ., και Κουτελιέρης, Φ.Α. (2008). *Προγραμματισμός Fortran 90/95 για επιστήμονες και μηχανικούς*, Εκδόσεις Τζιόλα, Αθήνα.

Παπαδόπυλος, Β. (1998*). Οριακή ανάλυση αξιοπιστίας τρισδιάστατων πλαισιακών κατασκευών με στοχαστικά πεπερασμένα στοιχεία, Διδακτορική Διατριβή*, ΕΜΠ.

Παπαδρακάκης, Μ. (1996). *Ανάλυση Φορέων με τη Μέθοδο των Πεπερασμένων Στοιχείων*, Εκδόσεις Παπασωτηρίου, Αθήνα.

Παπαδρακάκης, Μ. (1998). *Μη Γραμμικά Πεπερασμένα Στοιχεία, Σημειώσεις Μαθήματος*, ΕΜΠ, Αθήνα.